Chapter 3

TiO_2 : RE –Polyacrylic acid Nanocomposites

3.1 Introduction:

Rare earth doped transition metal oxide nanomaterials and oxide-polymer nanocomposites are gaining importance due to their novel properties. This study explores the properties of TiO_2 doped with rare earth elements and its composite with polyacrylic acid. There are several bottom-up and top-down methods to synthesize these materials [1-6]. Among these techniques, hydrothermal technique was used to synthesize RE doped TiO_2 in this work.

This chapter gives the process of synthesizing rare earth RE (Ce, Dy, Er, Eu, Pr, Tb, Tm) activated TiO_2 nano crystallites by hydrothermal technique with 0.1 mol% & 0.2 mol% doping concentration of rare earth elements. Fourteen such samples were synthesized and incorporated with polyacrylicacid (PAA) to develop thin films of polyacrylicacid-TiO_2:RE nanocomposites. The samples were characterized by various techniques, which are described in Chapter 2.

Hydrothermal Technique

Hydrothermal synthesis is known to yield materials with high crystallinity in various size and shape distributions. It is generally carried out in a stainless-steel autoclave with or without Teflon liners using water as one of the precursor solutions under controlled pressure and temperature. The reaction temperature can be raised above the boiling point, reaching the pressure of vapour saturation. The temperature and volume of precursor solution added to the autoclave defines the internal pressure produced. It is the most widely used method for the synthesis of nanomaterials and their characteristics can be modified by changing the parameters such as reaction temperature, reaction time, solvents and precursors used [7].

Technically, the term hydrothermal refers to any heterogeneous reaction in certain pressure and temperature conditions to dissolve and re-crystallize materials that are relatively insoluble under ordinary conditions. During re-crystallization, compounds with various structures and physical properties are formed. This affords excellent control over the morphology. The method can yield assorted nanostructures (e.g spheres, flowers, cubes, wires, tubes, etc.) with tenable size (from nm to microns) and uniformity [8].

Image of stainless steel autoclave for hydrothermal technique

3.2 Synthesis of Samples:

Precursors

Titanium(IV) Isopropoxide	$Ti\{OCH(CH_3)_2\}_4$
Cerium Nitrate Hexa Hydrate	$Ce(NO_3)_3.6H_2O$
Dysprosium Nitrate Hexa Hydrate	$Dy(NO_3)_3.6H_2O$
Erbium Nitrate Hexa Hydrate	$Er(NO_3)_3.6H_2O$
Europium Nitrate Hexa Hydrate	$Eu(NO_3)_3.6H_2O$
Praseodymium Nitrate Hexa Hydrate	$Pr(NO_3)_3.6H_2O$
Terbium Nitrate Hexa Hydrate	$Tb(NO_3)_3.6H_2O$
Thulium Nitrate Hexa Hydrate	$Tm(NO_3)_3.6H_2O$
De-Ionized Water	H_2O
Acrylicacid (Monomer)	$CH_2CHCOOH$
Potassium Persulfate (KPS)	$K_2S_2O_8$

All these chemicals are of analytical grade and used as received.

Preparation of RE (Ce, Dy, Er, Eu, Pr, Tb, Tm) doped TiO_2 nanoparticles

RE (Ce, Dy, Er, Eu, Pr, Tb, Tm) doped TiO_2 nanoparticles with 0.1 mol% & 0.2 mol% activator concentration of rare earth elements (for 30 mmol) were prepared by hydrothermal method. Fourteen such samples were synthesized. The process is shown in the flowchart given below.

Method of synthesis for 0.1 mol% and 0.2 mol% RE doped TiO_2 nanoparticles (RE=Ce, Dy, Er, Eu, Pr, Tb, Tm)

9.1 ml Ti – isopropoxide + 90 ml deionized water
+ $RE(NO_3)_3.6H_2O$(in stoichiometric proportions amounting to 0.1 mol% and 0.2 mol%)

↓

Stirring for 10 minutes at room temperature

↓

Solution transferred into stainless steel autoclave and kept into oven at 200°C for 2 hours and cooled naturally

↓

Resulting precipitates of TiO_2:RE filtered by Whatmann filter paper, washed with deionized water and Ethanol and dried at room temperature

↓

Dried material TiO_2:RE calcined at 400°C for 4 hours

↓

TiO_2:RE nanoparticles obtained after dried oxide material powdered with mortar and pestle

Image of stainless steel autoclave in oven used for synthesis

Preparation of polyacrylicacid- TiO_2:RE nanocomposites

Synthesized [RE (Ce, Dy, Er, Eu, Pr, Tb, Tm) doped TiO_2] samples were incorporated with polyacrylicacid (PAA) with 1 mol% & 2 mol% to develop thin films of the material. The process is shown in the flowchart given below. Fourteen samples were prepared using doctor blade method with uniform thickness for two different concentrations of the seven-doped samples shown in **Figure 3.1.**

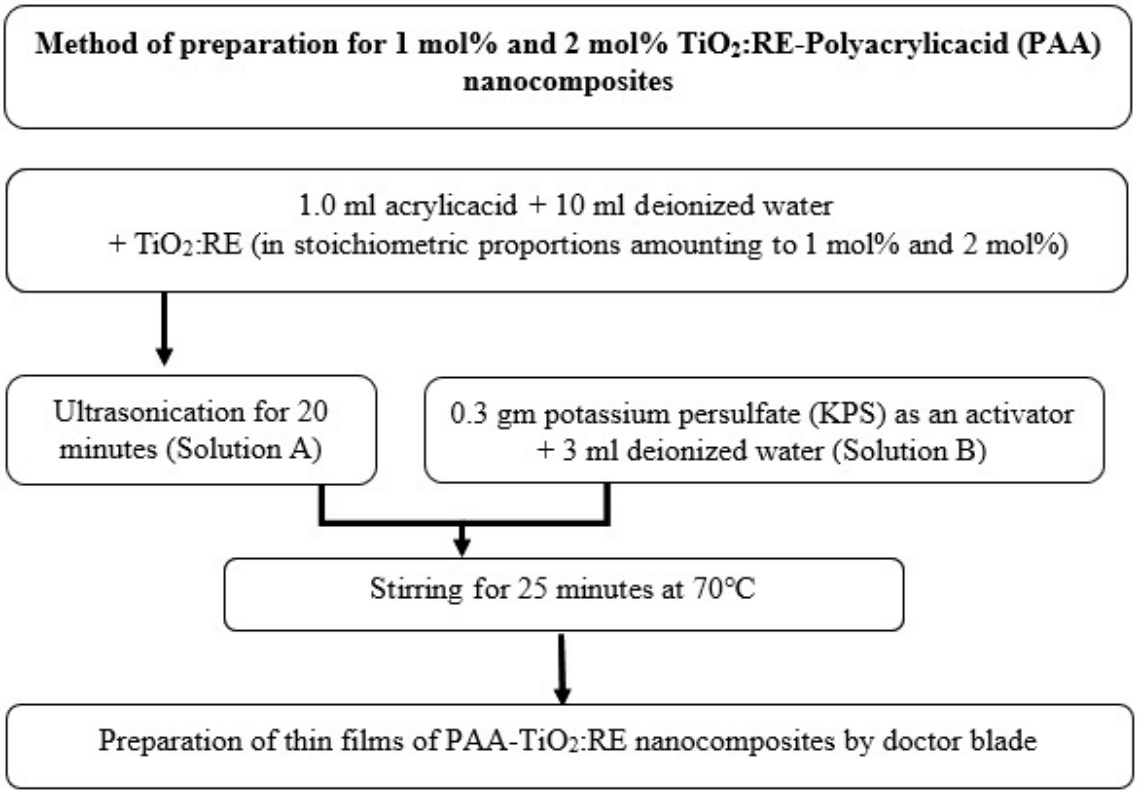

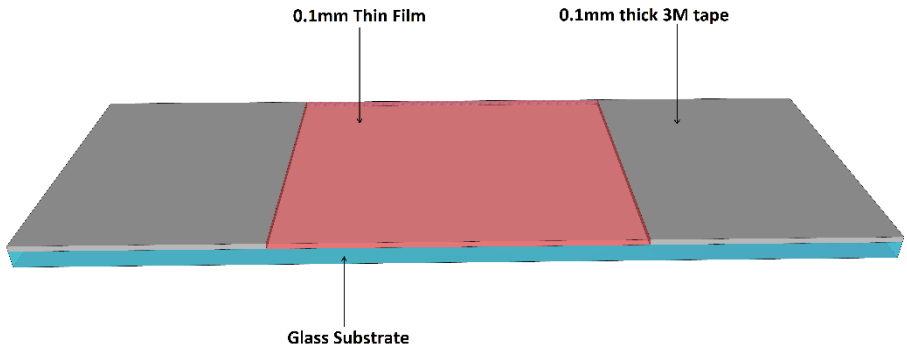

Figure 3.1: Illustration of the doctor blade method

Samples of the prepared nanocomposites are as under.

Table 3.1: Labelling of samples and their descriptions

Sample Label	Description
TCe1	0.1 mol% Ce doped TiO_2 nanoparticles
TDy1	0.1 mol% Dy doped TiO_2 nanoparticles
TEr1	0.1 mol% Er doped TiO_2 nanoparticles
TEu1	0.1 mol% Eu doped TiO_2 nanoparticles
TPr1	0.1 mol% Pr doped TiO_2 nanoparticles
TTb1	0.1 mol% Tb doped TiO_2 nanoparticles
TTm1	0.1 mol% Tm doped TiO_2 nanoparticles
TCe2	0.2 mol% Ce doped TiO_2 nanoparticles
TDy2	0.2 mol% Dy doped TiO_2 nanoparticles
TEr2	0.2 mol% Er doped TiO_2 nanoparticles
TEu2	0.2 mol% Eu doped TiO_2 nanoparticles
TPr2	0.2 mol% Pr doped TiO_2 nanoparticles
TTb2	0.2 mol% Tb doped TiO_2 nanoparticles
TTm2	0.2 mol% Tm doped TiO_2 nanoparticles
PTCe1	1 mol% TiO_2:Ce-PAA nanocomposites
PTDy1	1 mol% TiO_2:Dy-PAA nanocomposites
PTEr1	1 mol% TiO_2:Er-PAA nanocomposites
PTEu1	1 mol% TiO_2:Eu-PAA nanocomposites
PTPr1	1 mol% TiO_2:Pr-PAA nanocomposites
PTTb1	1 mol% TiO_2:Tb-PAA nanocomposites
PTTm1	1 mol% TiO_2:Tm-PAA nanocomposites
PTCe2	2 mol% TiO_2:Ce-PAA nanocomposites
PTDy2	2 mol% TiO_2:Dy-PAA nanocomposites
PTEr2	2 mol% TiO_2:Er-PAA nanocomposites
PTEu2	2 mol% TiO_2:Eu-PAA nanocomposites
PTPr2	2 mol% TiO_2:Pr-PAA nanocomposites
PTTb2	2 mol% TiO_2:Tb-PAA nanocomposites
PTTm2	2 mol% TiO_2:Tm-PAA nanocomposites

3.3 Characterization:

The structural and elemental properties of the powder samples were studied by X-Ray Diffraction (XRD), Energy Dispersive X-ray Spectroscopy (EDS) and Particle Size Analyzer (DLS). Fourier Transformation Infra-Red Spectroscopy (FTIR) studies the functional groups in the samples.

3.3.1 Structural and Elemental properties of powder nanoparticles (X-Ray Diffraction, Energy Dispersive X-ray Spectroscopy and Particle Size Analyzer)

X-ray powder diffraction of the powder samples was carried out on a GNR APD 2000 PRO X-Ray Diffractometer (XRD) at room temperature. The 2θ range was taken from 10° to 80° in scan mode with step increment of 0.020°.

The Energy Dispersive X-ray Spectroscopy (EDS) of the samples was carried out on a spectrometer attached to the Scanning Electron Microscope JEOL make JSM 5810 LV. The distribution of the hydrodynamic diameters of the nanoparticles were determined using a Malvern Nano ZS particle size analyzer by Dynamic Light Scattering (DLS) technique.

Figure 3.2(a) shows the XRD pattern of 0.1 mol% Ce doped TiO_2 nanoparticles (TCe1), which has sharp peaks. The pattern indicates high degree of crystallinity. These peaks are ascribed to TiO_2. The structure is predominantly in Anatase phase. The observed XRD peaks are indexed as (101), (004), (200), (211), (204), (220) and (215). They are in good agreement with JCPDS card no. 21-1272 shown in **Table 3.2** [9]. The peak at 2θ value of 25.50º has the highest intensity corresponding to (101) plane. The second highest value of intensity of 277.84 is seen at 2θ value of 48.10º, which is for (200) plane. Thereafter, third highest peak intensity observed at 2θ value of 37.83º is for (004) plane as shown in **Table 3.2**. The d-values of all the peaks match with those reported in the JCPDS card no. 21-1272 for TiO_2 anatase phase.

Figures 3.3(a) to **3.8(a)** show the XRD pattern for samples TRE1 (RE= Dy, Er, Eu, Pr, Tb, Tm). These patterns are identical to the XRD pattern of sample TCe1. They also indicate high degree of crystallinity. The peak at 2θ value around 25º has the highest intensity in all the samples, which is the characteristic peak of (101) plane. d-values of the peaks (101), (004), (200), (211), (204), (220) and (215) match with JCPDS card no. 21-1272 for TiO_2 anatase as shown in **Tables 3.3** to **3.8**.

There are no other peaks detected in these XRD patterns. It confirms the formation of material in pure form with good amount of crystallinity. The peaks are broad, which might be due to the formation of material in nano scale.

The average crystallite size of the samples are calculated by Scherrer formula [10]. The average crystallite size, evident from the broadening of XRD peaks, is found to be in nanometer. The calculated values are given in **Table 3.9**.

Figures 3.2(b) to **3.8(b)** show the EDS spectra of 0.1 mol% RE doped TiO_2 (TRE1) sample. They indicate the presence of Titanium, Oxygen and rare earth dopant. The results obtained from EDS are shown in **Table 3.11** in terms of Atomic%. It is observed that synthesized samples are slightly oxygen rich, which may be due to calcination of the samples.

The average diameter for 0.1 mol% RE doped TiO_2 (TRE1) samples dispersed in water were also measured using particle size analyzer by Dynamic Light Scattering (DLS) technique. **Figures 3.2(c)** to **3.8(c)** show the DLS results of the samples. The majority of the particles are distributed in the range of 24 nm to 49 nm. There is a short tail towards the larger particle size showing the residual particles. These larger particles could not be eliminated even after extended sonication. The distribution of diameter of the particles is shown in **Table 3.10**.

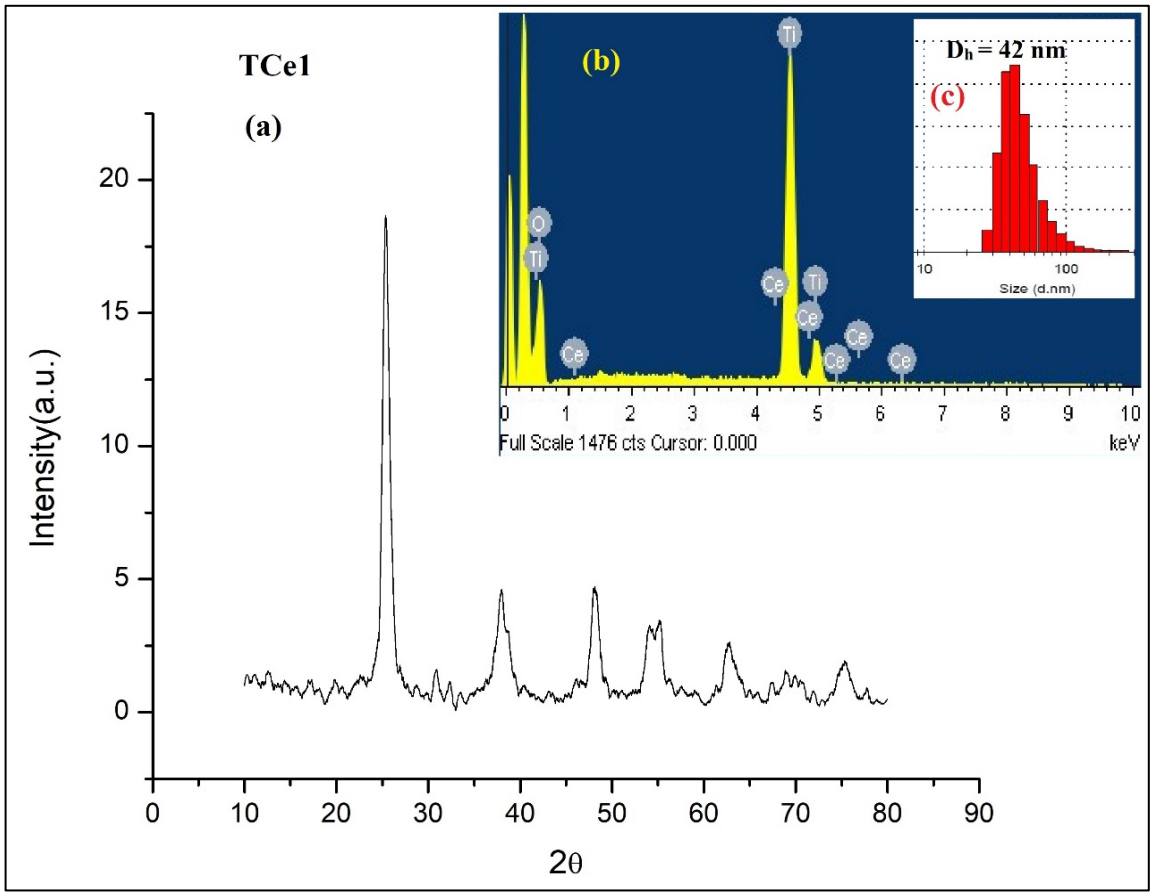

Figure 3.2: XRD pattern (a), EDS spectra (b) and DLS pattern (c) of TCe1

Table 3.2: Structural parameters of Ce doped TiO_2 sample (TCe1)

2θ TCe1	Intensity I/I0	Calculated d values	JCPDS 21-1272 d values	hkl
25.50	1000	3.5169	3.52	(101)
37.83	230.47	2.3785	2.378	(004)
48.10	277.84	1.8918	1.8920	(200)
55.17	198.31	1.6650	1.6665	(211)
62.55	132.06	1.4850	1.4808	(204)
70.74	86.22	1.3318	1.3378	(220)
74.79	114.62	1.2694	1.2649	(215)

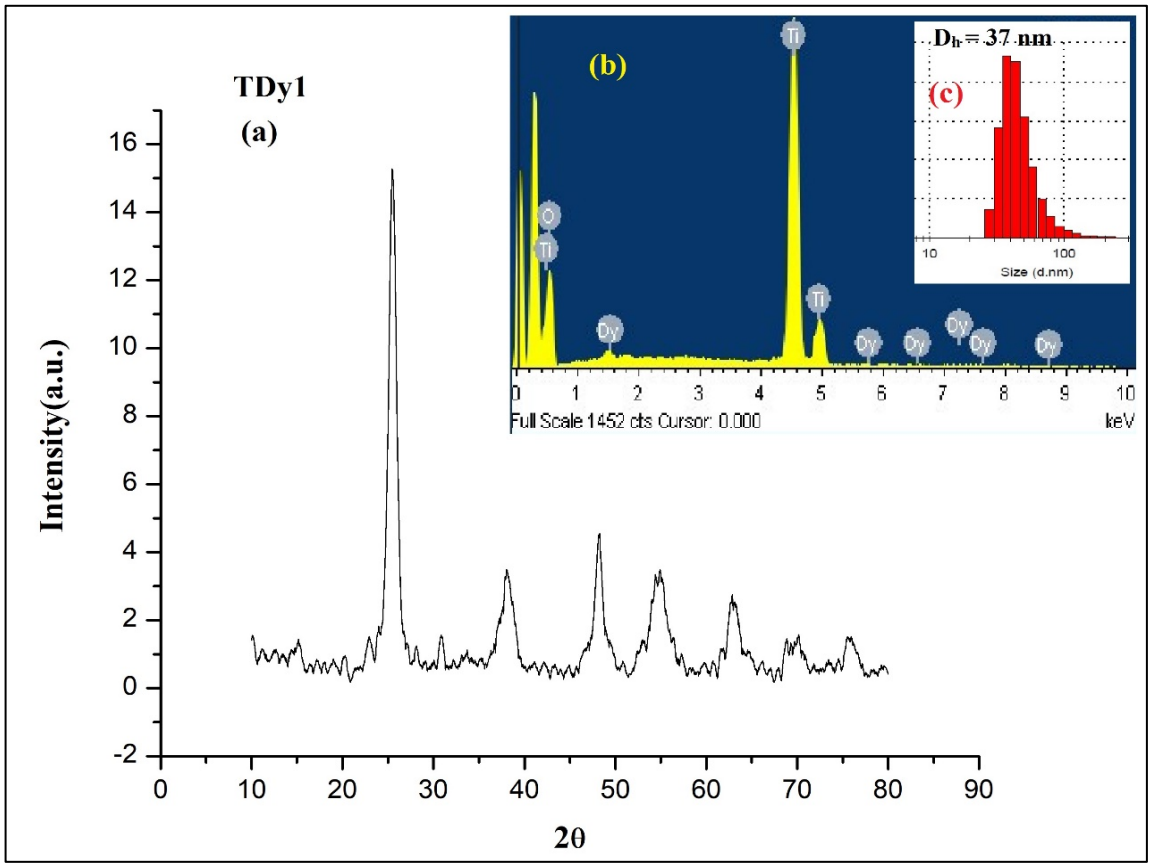

Figure 3.3: XRD pattern (a), EDS spectra (b) and DLS pattern (c) of TDy1

Table 3.3: Structural parameters of Dy doped TiO_2 sample (TDy1)

2θ TDy1	Intensity I/I0	Calculated d values	JCPDS 21-1272 d values	hkl
25.52	1000	3.5039	3.52	(101)
38.13	232.62	2.3603	2.378	(004)
48.28	317.22	1.8850	1.8920	(200)
55.06	237.86	1.6680	1.6665	(211)
63.02	157.28	1.4751	1.4808	(204)
70.29	122.29	1.3392	1.3378	(220)
75.35	120.97	1.2614	1.2649	(215)

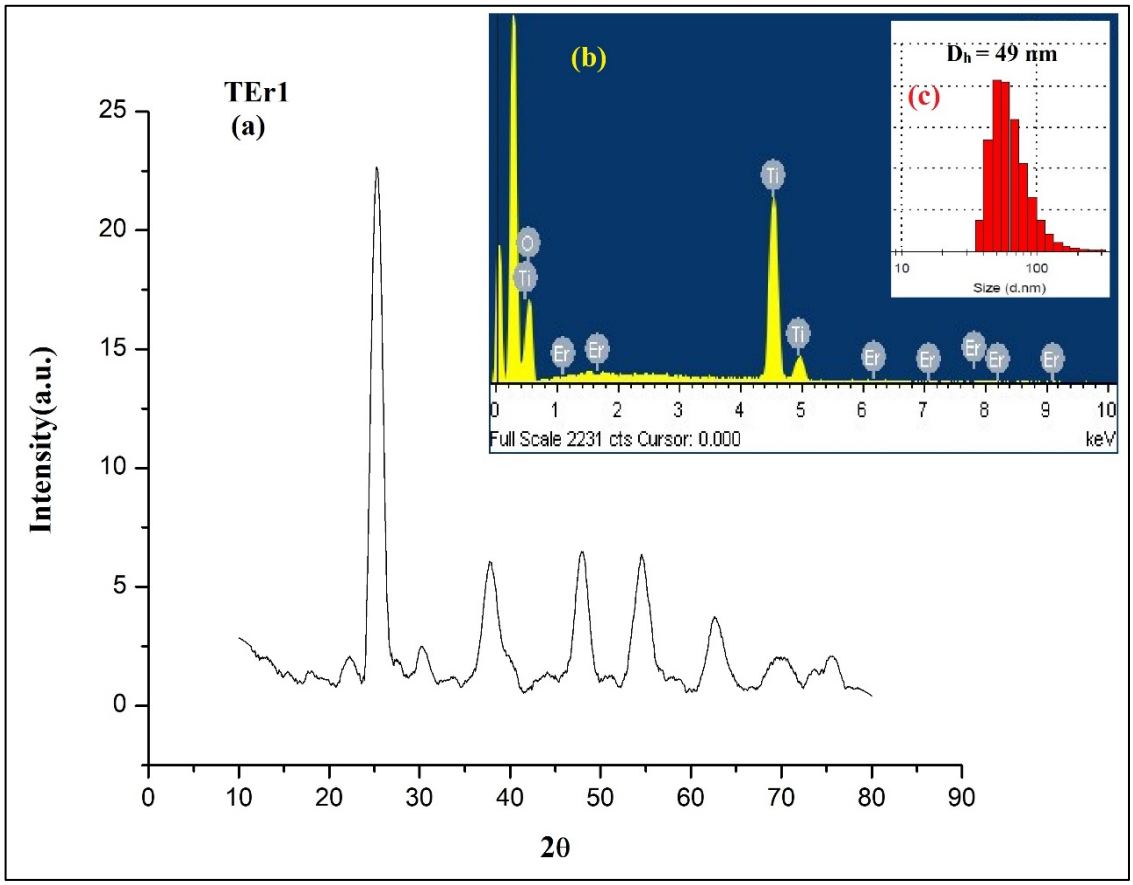

Figure 3.4: XRD pattern (a), EDS spectra (b) and DLS pattern (c) of TEr1

Table 3.4: Structural parameters of Er doped TiO_2 sample (TEr1)

2θ TEr1	Intensity I/I0	Calculated d values	JCPDS 21-1272 d values	hkl
25.17	1000	3.5382	3.52	(101)
37.92	210.39	2.3727	2.378	(004)
47.91	231.56	1.8988	1.8920	(200)
54.87	214.45	1.6734	1.6665	(211)
62.62	129.22	1.4835	1.4808	(204)
70.25	75.97	1.3399	1.3378	(220)
75.49	56.56	1.2594	1.2649	(215)

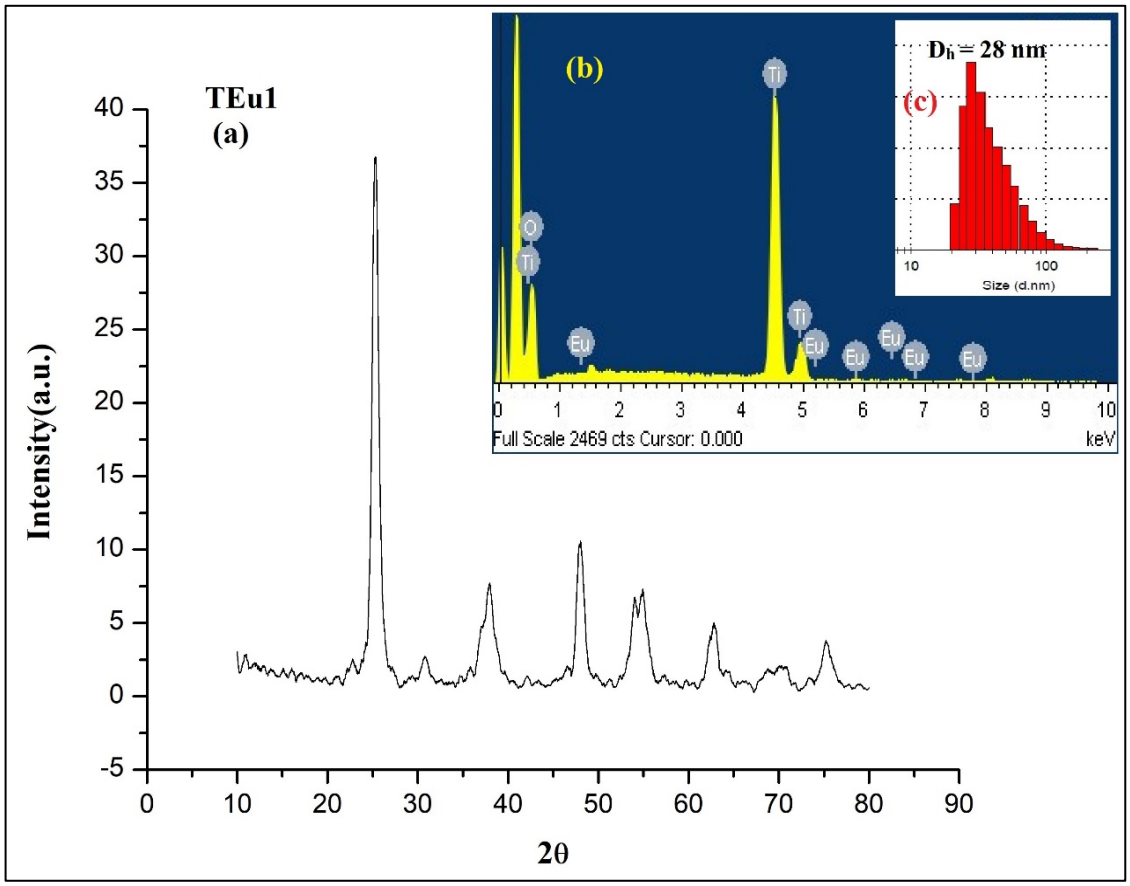

Figure 3.5: XRD pattern (a), EDS spectra (b) and DLS pattern (c) of TEu1

Table 3.5: Structural parameters of Eu doped TiO_2 sample (TEu1)

2θ TEu1	Intensity I/I0	Calculated d values	JCPDS 21-1272 d values	hkl
25.26	1000	3.5237	3.52	(101)
38.32	201.68	2.3748	2.378	(004)
47.65	259.47	1.8817	1.8920	(200)
54.73	212.56	1.6752	1.6665	(211)
62.79	149.45	1.4867	1.4808	(204)
70.38	55.32	1.3321	1.3378	(220)
75.36	96.74	1.2586	1.2649	(215)

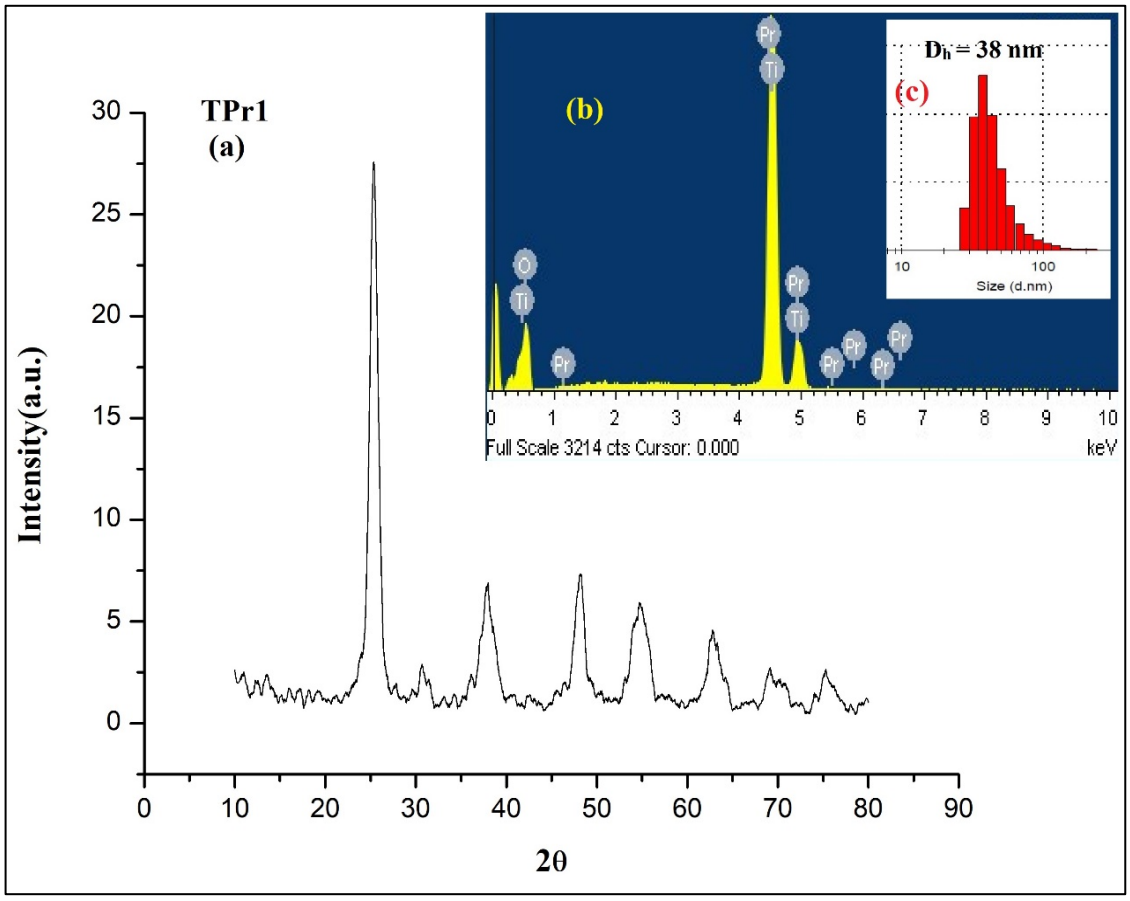

Figure 3.6: XRD pattern (a), EDS spectra (b) and DLS pattern (c) of TPr1

Table 3.6: Structural parameters of Pr doped TiO_2 sample (TPr1)

2θ TPr1	Intensity I/I0	Calculated d values	JCPDS 21-1272 d values	hkl
25.38	1000	3.5376	3.52	(101)
37.45	265.69	2.3825	2.378	(004)
47.83	251.88	1.8865	1.8920	(200)
54.61	195.73	1.6621	1.6665	(211)
63.27	183.17	1.4723	1.4808	(204)
70.54	104.83	1.3312	1.3378	(220)
75.64	106.16	1.2618	1.2649	(215)

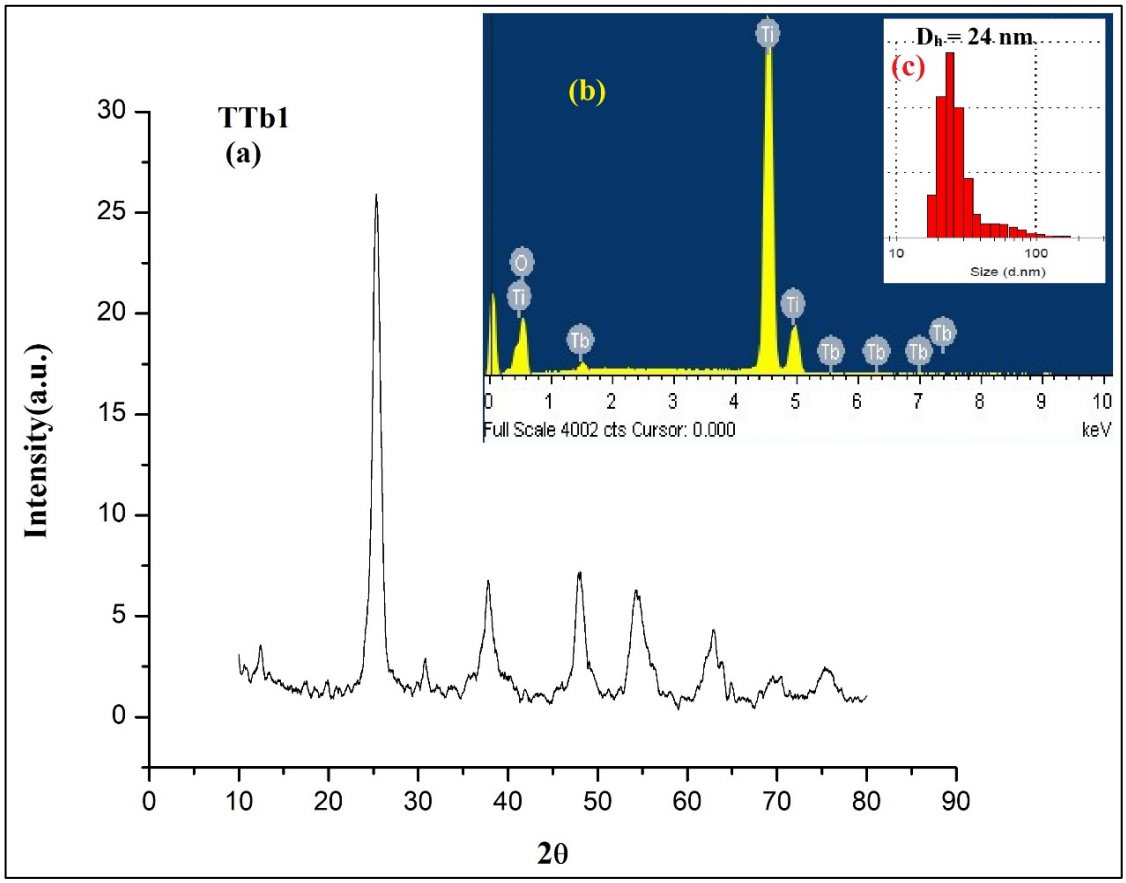

Figure 3.7: XRD pattern (a), EDS spectra (b) and DLS pattern (c) of TTb1

Table 3.7: Structural parameters of Tb doped TiO_2 sample (TTb1)

2θ TTb1	Intensity I/I0	Calculated d values	JCPDS 21-1272 d values	hkl
25.65	1000	3.5165	3.52	(101)
37.76	219.12	2.3679	2.378	(004)
48.23	231.45	1.8973	1.8920	(200)
55.17	208.67	1.6638	1.6665	(211)
62.61	138.14	1.4874	1.4808	(204)
70.21	70.18	1.3428	1.3378	(220)
75.28	95.76	1.2631	1.2649	(215)

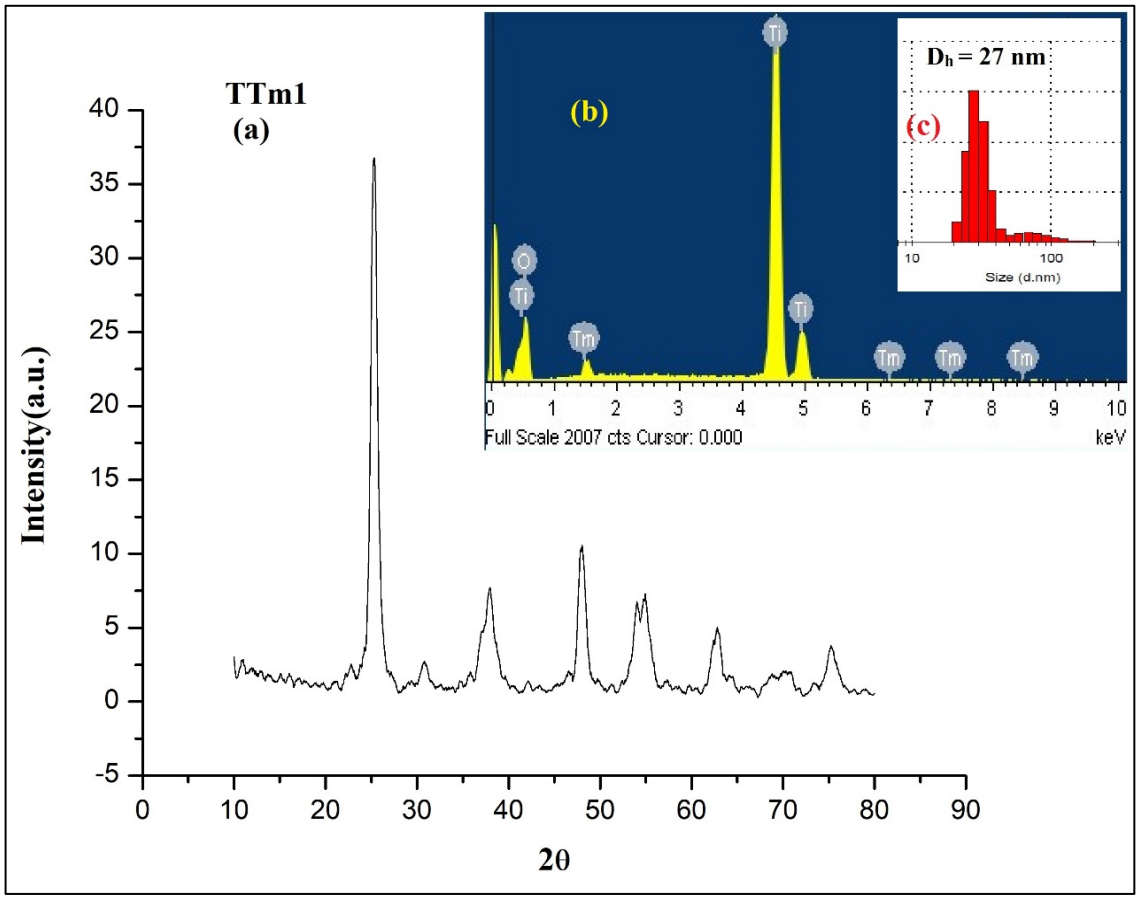

Figure 3.8: XRD pattern (a), EDS spectra (b) and DLS pattern (c) of TTm1

Table 3.8: Structural parameters of Tm doped TiO_2 sample (TTm1)

2θ TTm1	Intensity I/I0	Calculated d values	JCPDS 21-1272 d values	hkl
25.25	1000	3.5274	3.52	(101)
37.92	202.75	2.3728	2.378	(004)
47.88	260.08	1.9000	1.8920	(200)
54.85	213.50	1.6739	1.6665	(211)
62.96	150.39	1.4784	1.4808	(204)
70.10	54.25	1.3423	1.3378	(220)
75.15	96.86	1.2602	1.2649	(215)

The average crystallite sizes, thus calculated and given in **Table 3.9**. The results clearly indicate that the samples are in nanocrystalline phase, and the crystallite size varies from 5.83 nm to 8.20 nm.

Table 3.9: Crystallite size for TRE1 (RE= Ce, Dy, Er, Eu, Pr, Tb, Tm) samples

Sample	Crystallite Size (nm)
TCe1	**7.49**
TDy1	**7.95**
TEr1	**6.03**
TEu1	**5.83**
TPr1	**6.86**
TTb1	**8.20**
TTm1	**6.13**

Table 3.10: Distribution of Diameter of TRE1 samples

Sample	Diameter D_h (nm)
TCe1	**42**
TDy1	**37**
TEr1	**49**
TEu1	**28**
TPr1	**38**
TTb1	**24**
TTm1	**27**

Table 3.11: Elemental composition of TRE1 samples obtained from EDS

Sample	Atomic %	
	Ti	O
TCe1	21.28	78.58
TDy1	22.37	77.47
TEr1	21.11	78.74
TEu1	25.13	74.71
TPr1	26.70	73.17
TTb1	27.78	72.10
TTm1	28.44	71.43

The XRD patterns of 0.2 mol% RE doped TiO_2 nanoparticles (TRE2) are shown in **Figures 3.9(a)** to **3.15(a).** The structural parameters are given in **Tables 3.12** to **3.18**.

Figures 3.9(a) to **3.15(a)** represent the XRD pattern for TRE2 (RE= Ce, Dy, Er, Eu, Pr, Tb, Tm) samples. They are quite identical with each other and to the XRD pattern of TRE1 samples as well. The only exception is the disappearance of the peak at 2θ value around 55º of (211) plane [in TRE1] and appearance of (105) plane [in TRE2]. The peak at 2θ value around 25º has the highest intensity in all the samples, which is the characteristic peak of (101) plane. d-values of the peaks (101), (004), (200), (105), (204), (220) and (215) match with JCPDS card no. 21-1272 for TiO_2 anatase as shown in **Tables 3.12** to **3.18** [9]. The peaks are seen to be slightly broadened with higher doping concentration. This may be due to the consequences of mismatch of the radius of dopant and host ion.

The average crystallite size for TiO_2:RE samples with 0.2 mol% doping concentration of rare earth elements (TRE2) are given in **Table 3.19**.

Figures 3.9(b) to **3.15(b)** show the EDS spectra of 0.2 mol% RE doped TiO_2 (TRE2) sample which indicates the presence of Titanium, Oxygen and rare earth elements thus showing the purity of the sample. The results of EDS are shown in **Table 3.21** in terms of Atomic%. It is observed that synthesized samples are slightly oxygen rich which may be due to calcination of the samples.

The average diameter (D_h) for 0.2 mol% RE doped TiO_2 (TRE2) samples dispersed in water were also measured using particle size analyzer by dynamic light scattering (DLS) technique. **Figures 3.9(c)** to **3.15(c)** show the DLS results of TRE2 samples indicating the range of distribution for all samples is 27-57 nm with a short tail towards the larger particle size. The larger particles not being eliminated even after extension of sonication. The distribution of diameter of the particles are found in nanometer range as shown in **Table 3.20**.

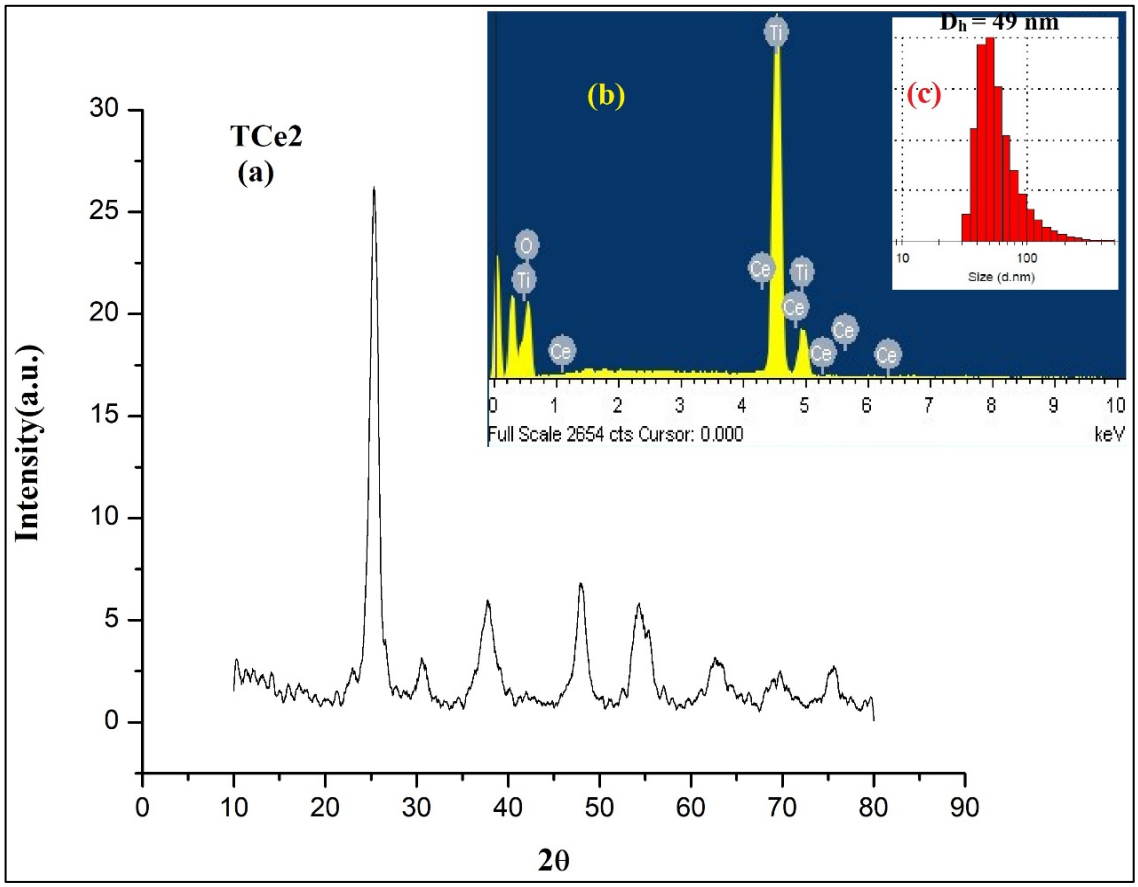

Figure 3.9: XRD pattern (a), EDS spectra (b) and DLS pattern (c) of TCe2

Table 3.12: Structural parameters of Ce doped TiO_2 sample (TCe2)

2θ TCe2	Intensity I/I0	Calculated d values	JCPDS 21-1272 d values	hkl
25.43	1000	3.5027	3.52	(101)
38.03	208.23	2.3660	2.378	(004)
47.95	284.79	1.8972	1.8920	(200)
54.10	243.82	1.6951	1.6999	(105)
62.90	118.78	1.4775	1.4808	(204)
69.74	104.46	1.3464	1.3378	(220)
75.65	88.03	1.2572	1.2649	(215)

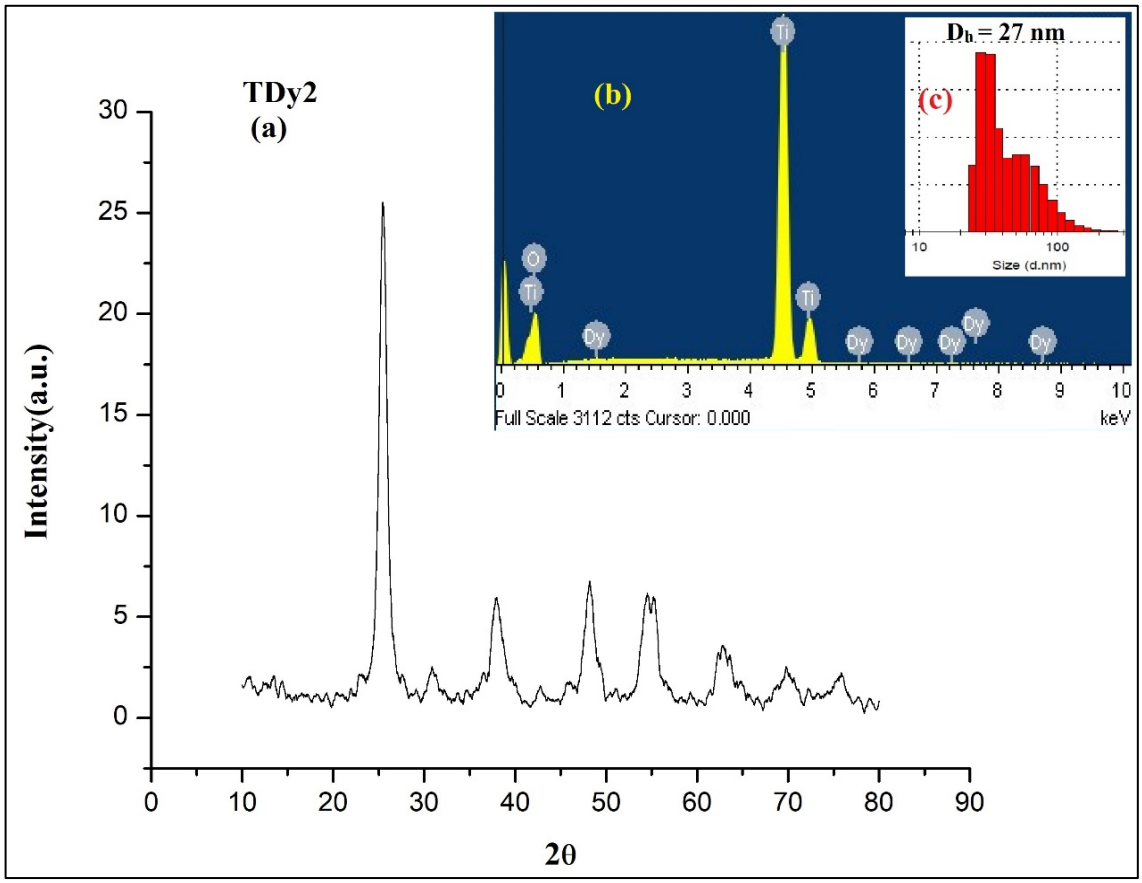

Figure 3.10: XRD pattern (a), EDS spectra (b) and DLS pattern (c) of TDy2

Table 3.13: Structural parameters of Dy doped TiO_2 sample (TDy2)

2θ TDy2	Intensity I/I0	Calculated d values	JCPDS 21-1272 d values	hkl
25.51	1000	3.5040	3.52	(101)
38.04	241.97	2.3658	2.378	(004)
47.90	233.20	1.8992	1.8920	(200)
54.48	235.34	1.6892	1.6999	(105)
63.00	150.36	1.4797	1.4808	(204)
70.02	91.28	1.3438	1.3378	(220)
75.28	70.81	1.2595	1.2649	(215)

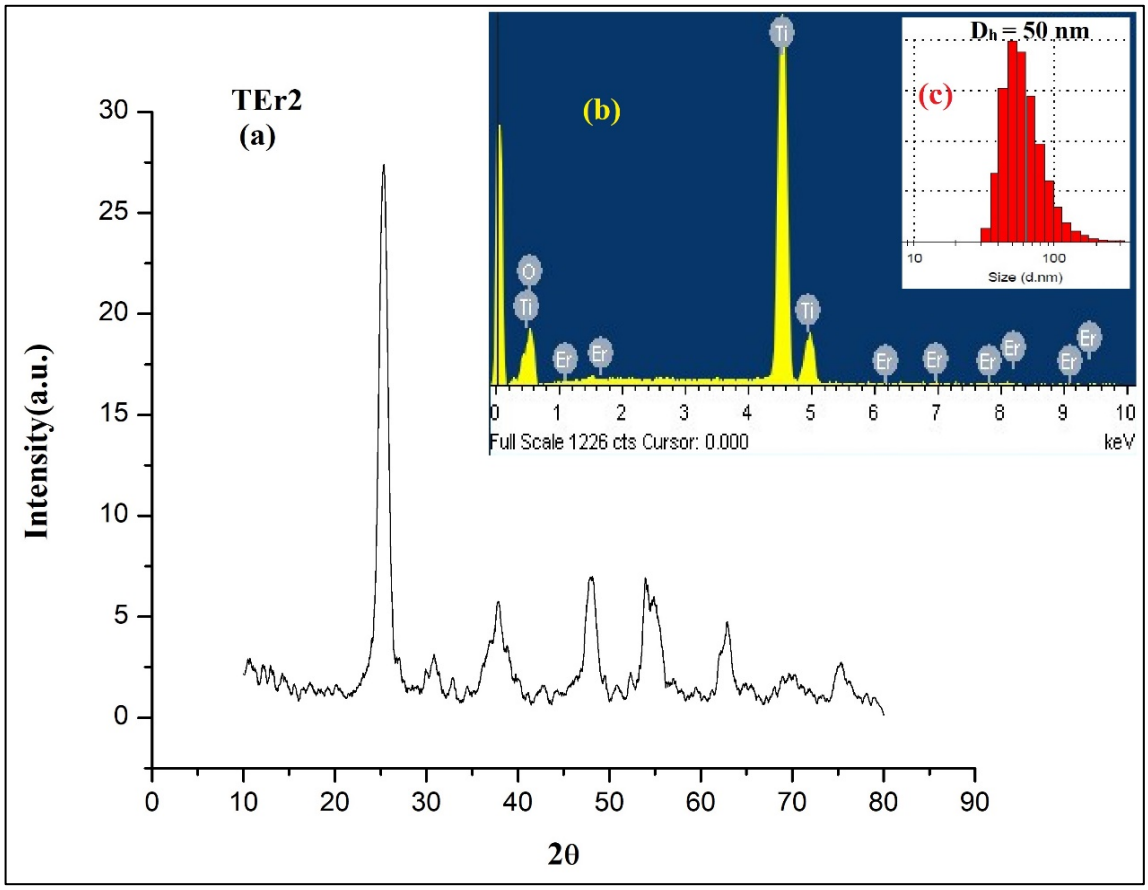

Figure 3.11: XRD pattern (a), EDS spectra (b) and DLS pattern (c) of TEr2

Table 3.14: Structural parameters of Er doped TiO_2 sample (TEr2)

2θ TEr2	Intensity I/I0	Calculated d values	JCPDS 21-1272 d values	hkl
25.28	1000	3.5230	3.52	(101)
38.00	219.58	2.3679	2.378	(004)
48.10	292.31	1.8918	1.8920	(200)
53.90	264.05	1.7010	1.6999	(105)
63.04	171.04	1.4799	1.4808	(204)
70.34	96.10	1.3383	1.3378	(220)
75.28	115.17	1.2589	1.2649	(215)

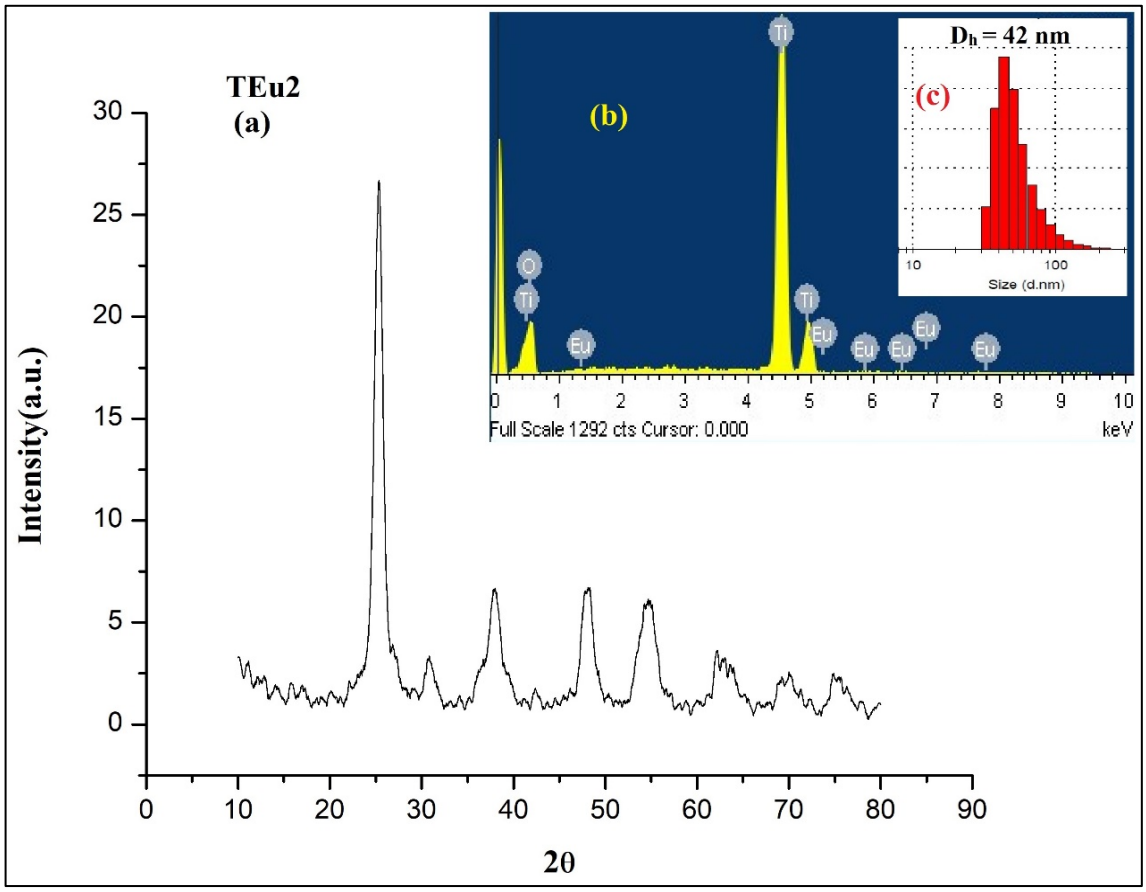

Figure 3.12: XRD pattern (a), EDS spectra (b) and DLS pattern (c) of TEu2

Table 3.15: Structural parameters of Eu doped TiO_2 sample (TEu2)

2θ TEu2	Intensity I/I0	Calculated d values	JCPDS 21-1272 d values	hkl
25.38	1000	3.5323	3.52	(101)
37.92	240.21	2.3730	2.378	(004)
48.06	269.89	1.8931	1.8920	(200)
54.47	250.89	1.6908	1.6999	(105)
62.89	151.50	1.4778	1.4808	(204)
70.09	111.57	1.3426	1.3378	(220)
75.10	94.73	1.2598	1.2649	(215)

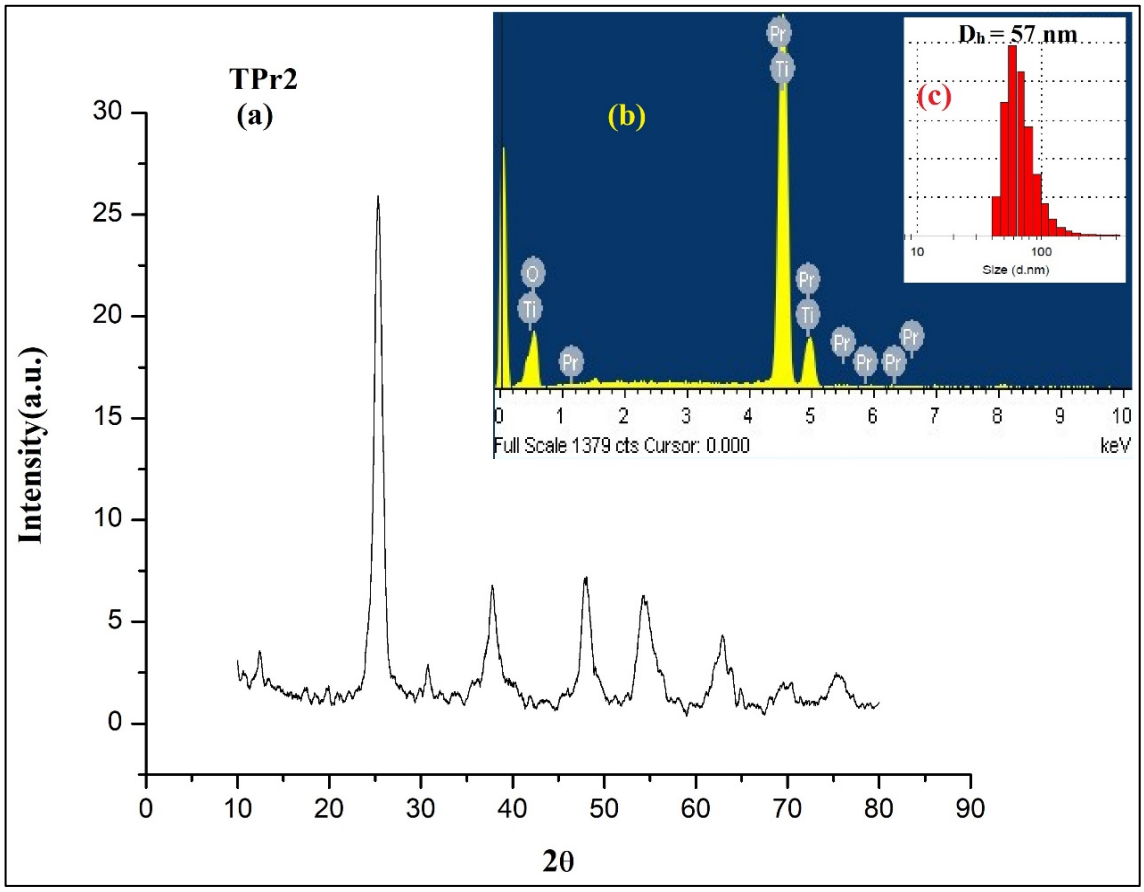

Figure 3.13: XRD pattern (a), EDS spectra (b) and DLS pattern (c) of TPr2

Table 3.16: Structural parameters of Pr doped TiO_2 sample (TPr2)

2θ TPr2	Intensity I/I0	Calculated d values	JCPDS 21-1272 d values	hkl
25.32	1000	3.5175	3.52	(101)
37.90	219.69	2.3741	2.378	(004)
47.96	232.17	1.8971	1.8920	(200)
53.98	209.45	1.6986	1.6999	(105)
63.06	138.63	1.4767	1.4808	(204)
70.17	71.84	1.3413	1.3378	(220)
75.33	95.94	1.2586	1.2649	(215)

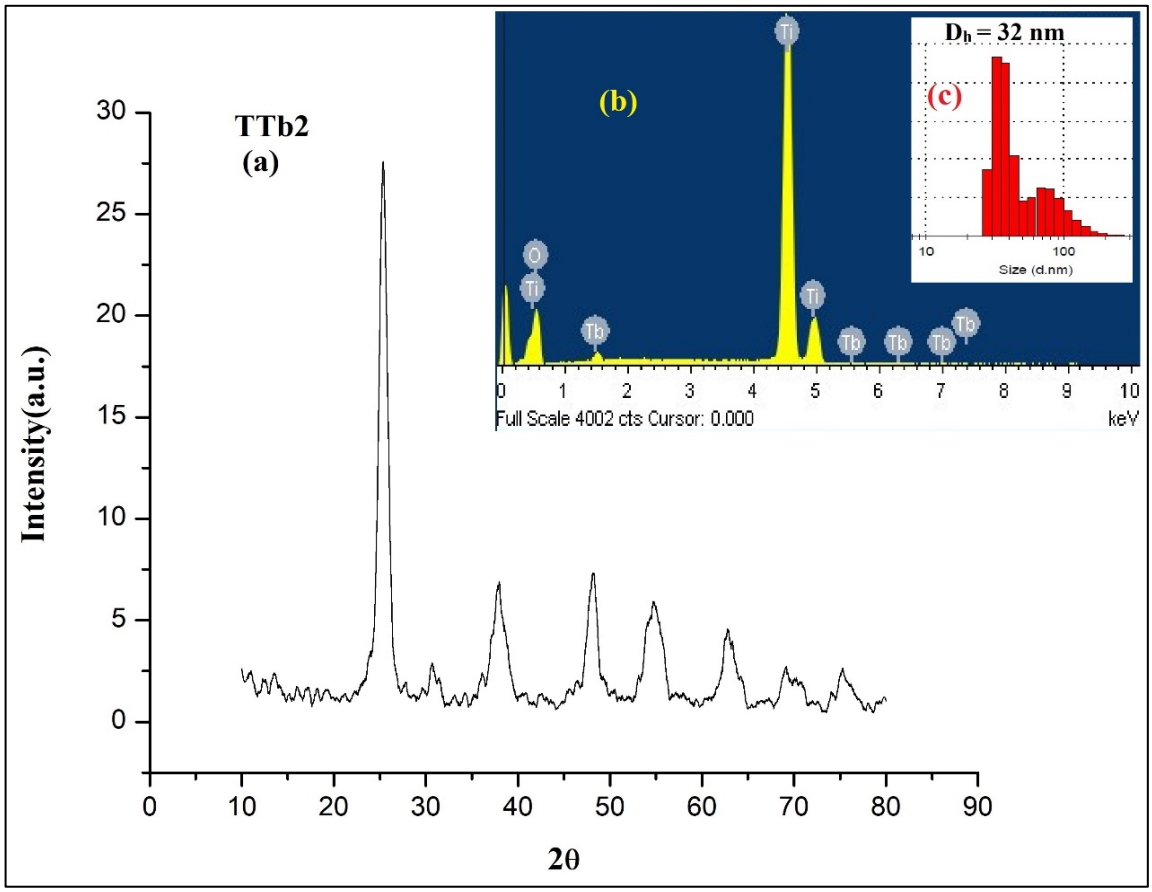

Figure 3.14: XRD pattern (a), EDS spectra (b) and DLS pattern (c) of TTb2

Table 3.17: Structural parameters of Tb doped TiO_2 sample (TTb2)

2θ TTb2	Intensity I/I0	Calculated d values	JCPDS 21-1272 d values	hkl
25.41	1000	3.5276	3.52	(101)
37.99	266.68	2.3689	2.378	(004)
48.25	252.68	1.8969	1.8920	(200)
54.44	196.34	1.6855	1.6999	(105)
62.68	183.76	1.4823	1.4808	(204)
69.35	105.10	1.3452	1.3378	(220)
74.99	106.74	1.2665	1.2649	(215)

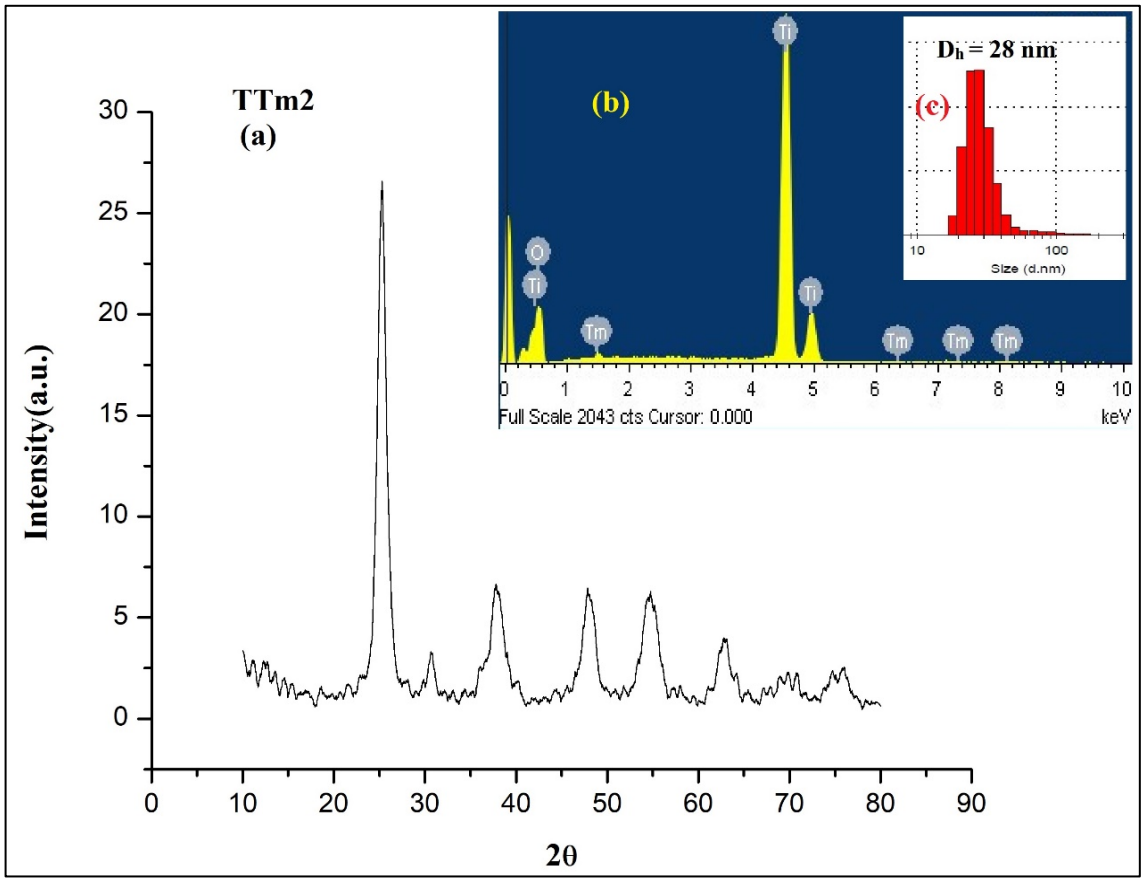

Figure 3.15: XRD pattern (a), EDS spectra (b) and DLS pattern (c) of TTm2

Table 3.18: Structural parameters of Tm doped TiO_2 sample (TTm2)

2θ TTm2	Intensity I/I0	Calculated d values	JCPDS 21-1272 d values	hkl
25.38	1000	3.5091	3.52	(101)
37.88	271.64	2.3752	2.378	(004)
47.93	259.38	1.8981	1.8920	(200)
54.22	223.99	1.6916	1.6999	(105)
62.84	126.60	1.4789	1.4808	(204)
70.71	73.26	1.3323	1.3378	(220)
74.75	73.49	1.2700	1.2649	(215)

Table 3.19: Crystallite size for TRE2 (RE= Ce, Dy, Er, Eu, Pr, Tb, Tm) samples

Sample	Crystallite Size (nm)
TCe2	6.74
TDy2	7.91
TEr2	5.22
TEu2	5.53
TPr2	6.16
TTb2	7.36
TTm2	5.83

Table 3.20: Distribution of Diameter of TRE2 samples

Sample	Diameter D_h (nm)
TCe2	49
TDy2	27
TEr2	50
TEu2	42
TPr2	57
TTb2	32
TTm2	28

Table 3.21: Elemental composition of TRE2 samples obtained from EDS

Sample	Atomic %	
	Ti	O
TCe2	29.00	70.79
TDy2	28.78	71.03
TEr2	29.31	70.44
TEu2	29.24	70.57
TPr2	29.17	70.49
TTb2	27.53	72.29
TTm2	27.32	72.38

Study of Composites

Samples

1. **1 mol% of RE doped TiO_2 blended with PAA(Poly Acrylic Acid)**
2. **2 mol% of RE doped TiO_2 blended with PAA(Poly Acrylic Acid)**

3.3.2 Fourier Transformation Infra-Red Spectroscopy (FTIR)

FTIR spectroscopic studies were done using JASCO FT/IR-4700 spectrometer recorded in the range 500-4000 cm^{-1}. FTIR spectra of pure PAA and 1 mol% TiO_2:RE – PAA nanocomposites (PTRE1) are shown in **Figures 3.16** to **3.23**. FTIR spectra of 2 mol% TiO_2:RE – PAA nanocomposites (PTRE2) are shown in **Figures 3.24** to **3.30**. The presence of different functional groups with respective wavenumber is shown in **Table 3.22**.

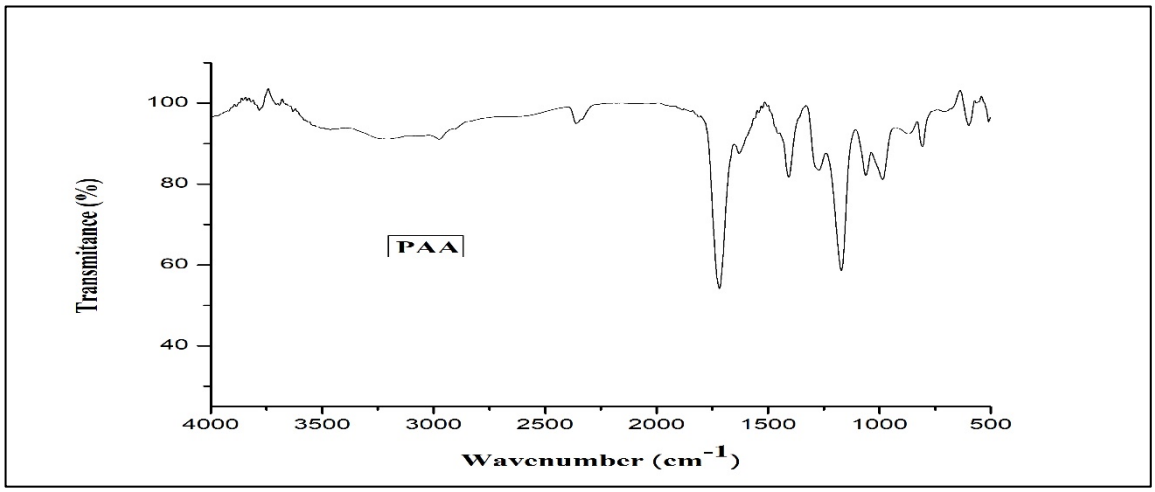

Figure 3.16: FTIR spectra of pure PAA

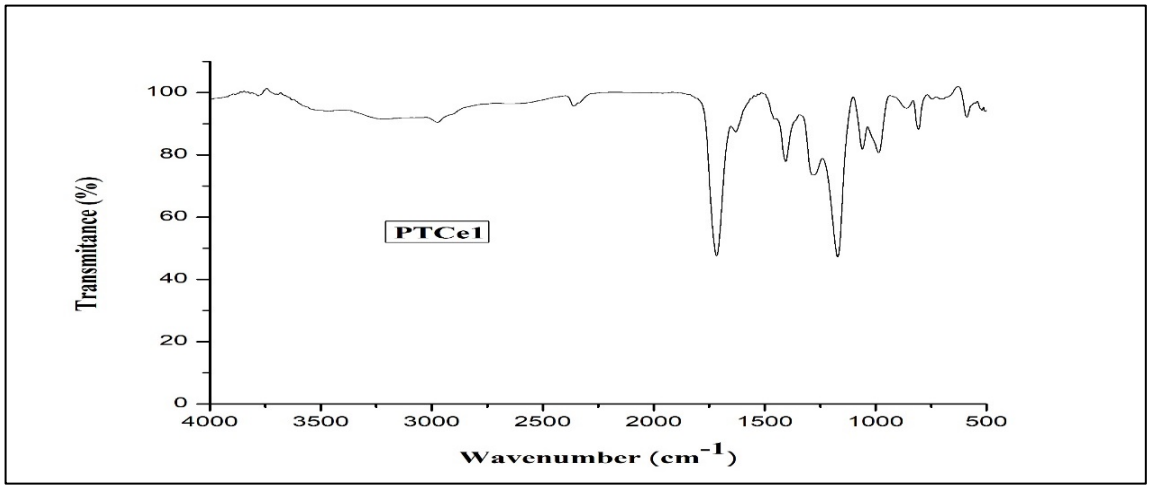

Figure 3.17: FTIR spectra of PTCe1 sample

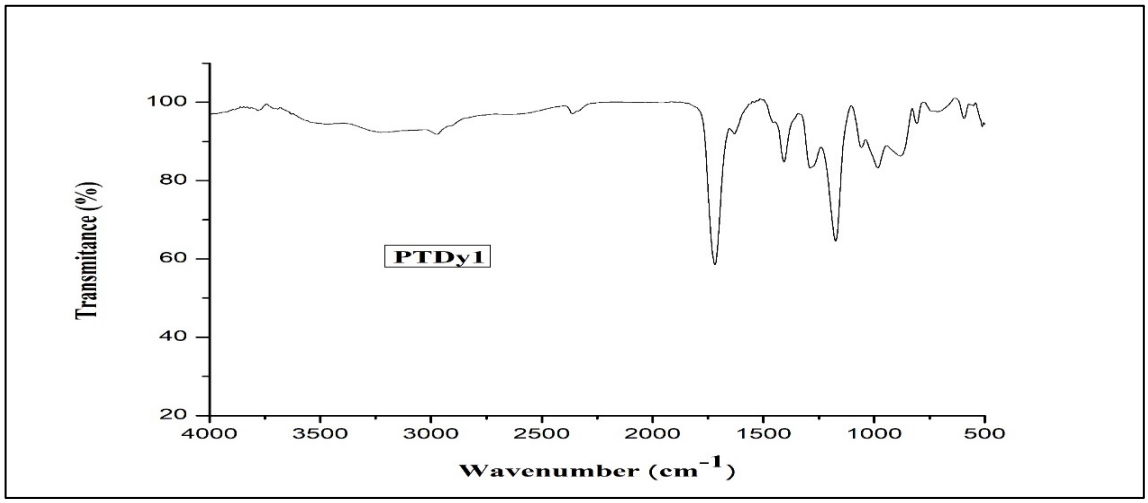

Figure 3.18: FTIR spectra of PTDy1 sample

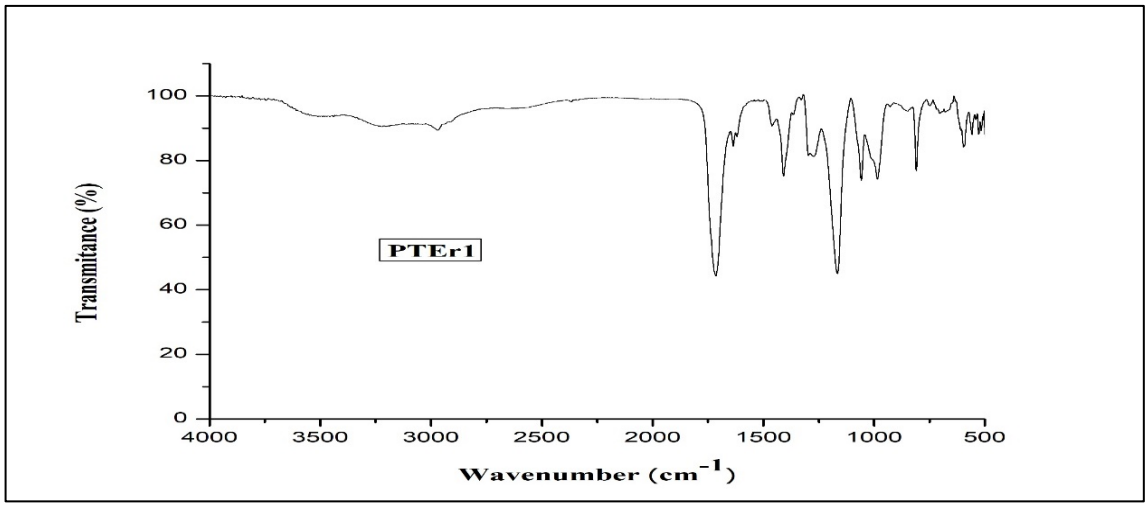

Figure 3.19: FTIR spectra of PTEr1 sample

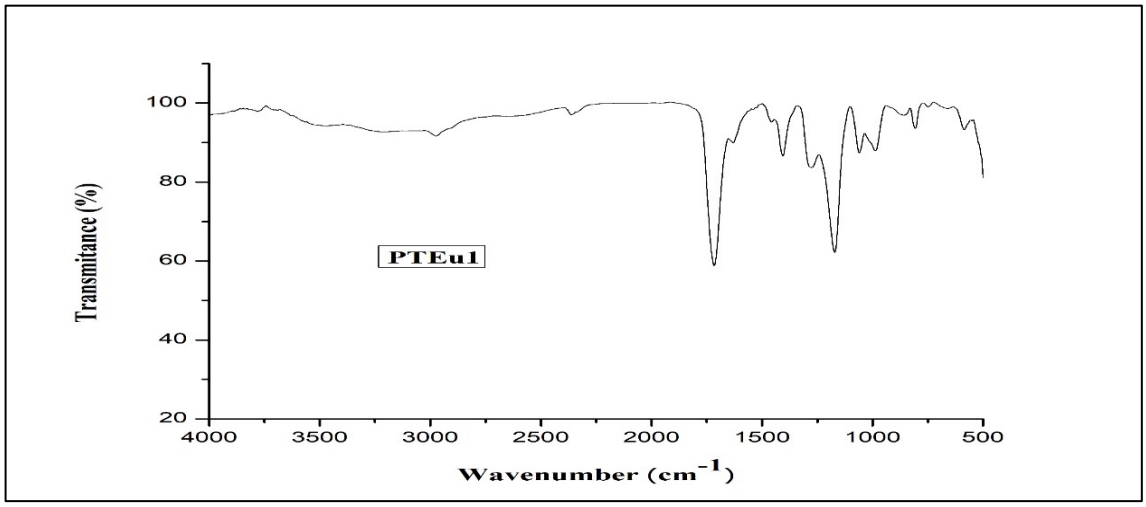

Figure 3.20: FTIR spectra of PTEu1 sample

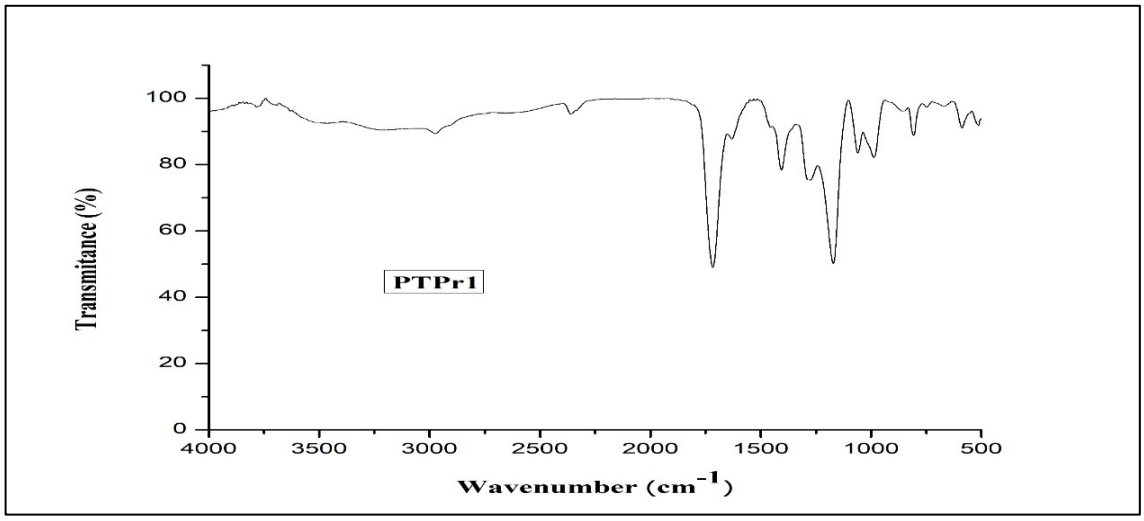

Figure 3.21: FTIR spectra of PTPr1 sample

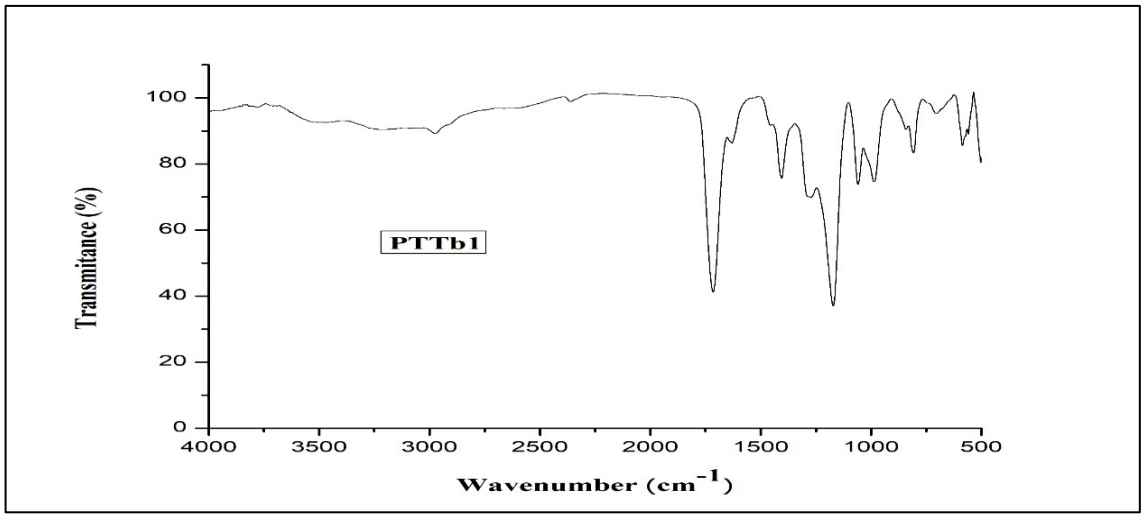

Figure 3.22: FTIR spectra of PTTb1 sample

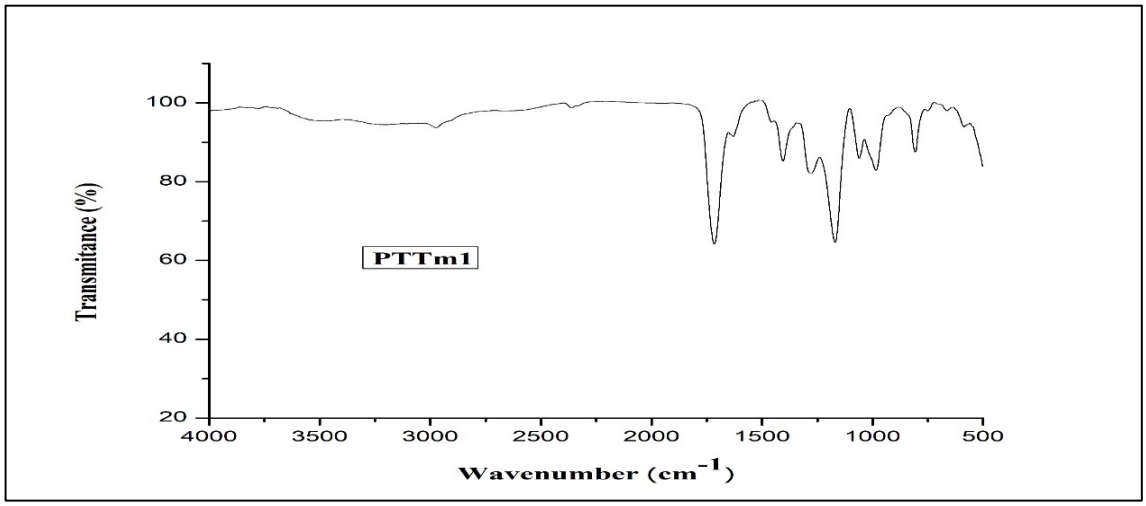

Figure 3.23: FTIR spectra of PTTm1 sample

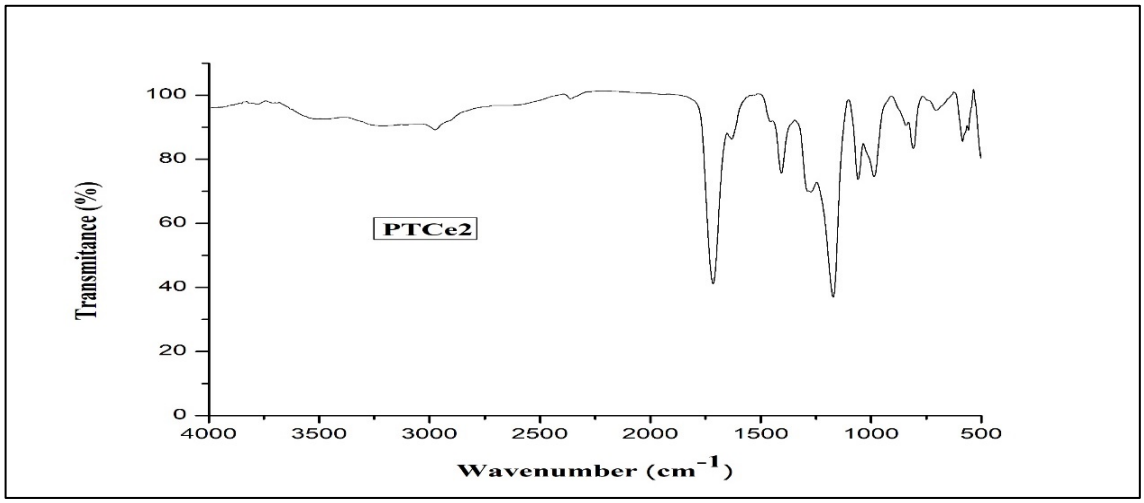

Figure 3.24: FTIR spectra of PTCe2 sample

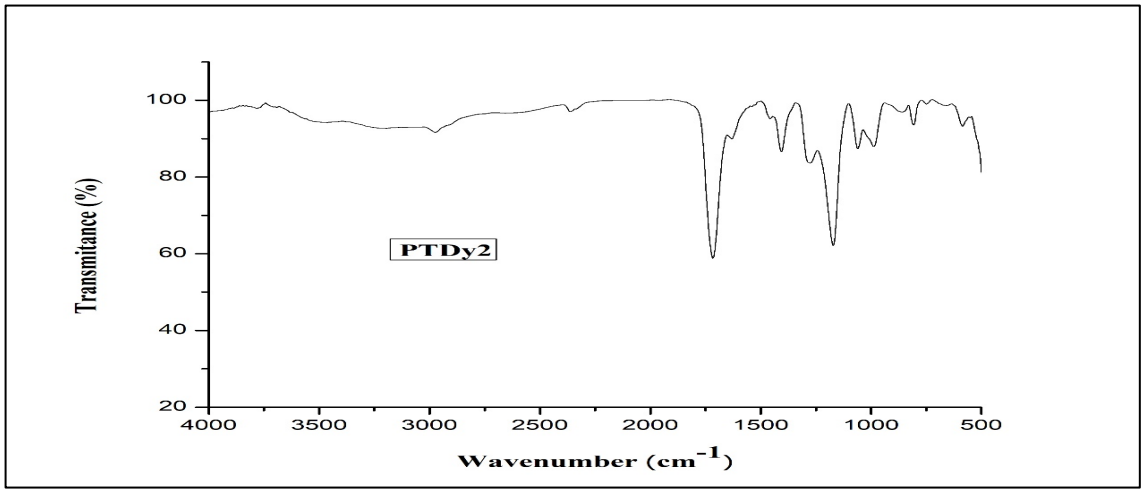

Figure 3.25: FTIR spectra of PTDy2 sample

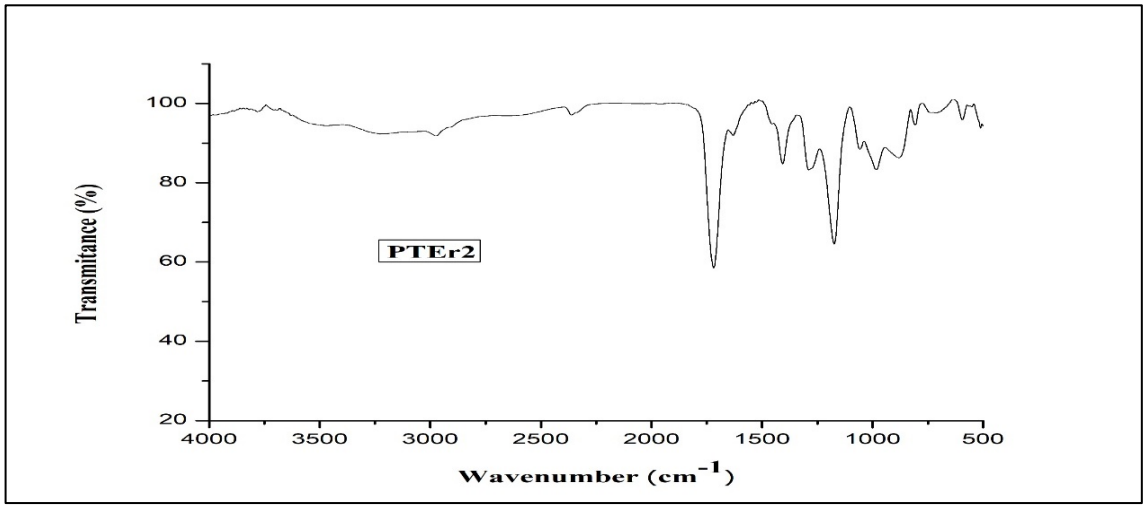

Figure 3.26: FTIR spectra of PTEr2 sample

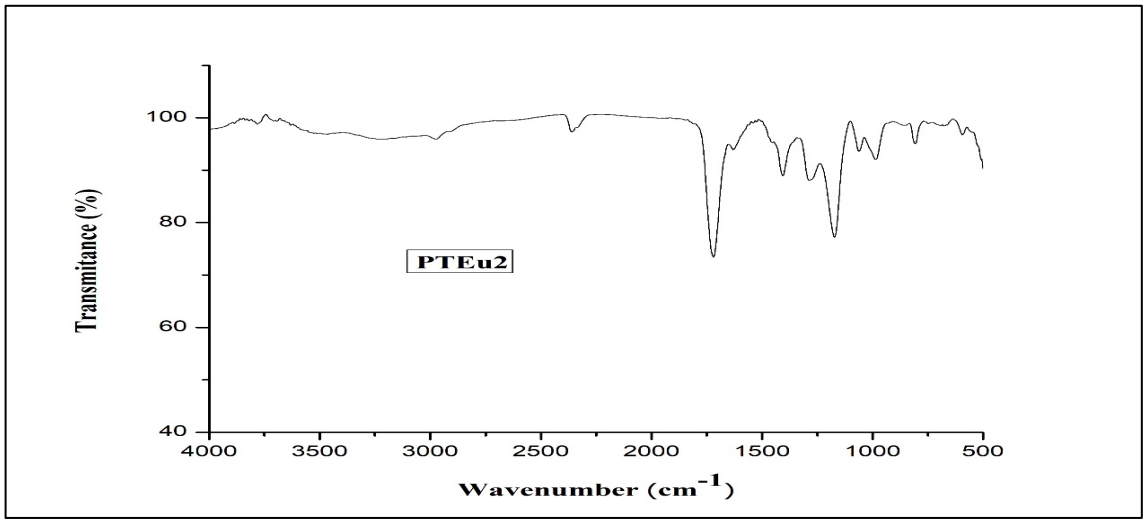

Figure 3.27: FTIR spectra of PTEu2 sample

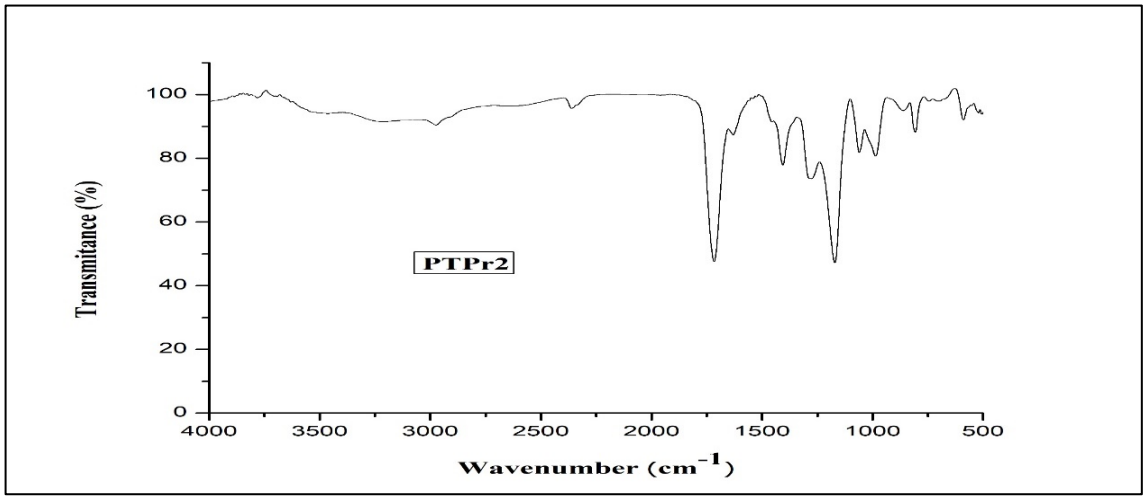

Figure 3.28: FTIR spectra of PTPr2 sample

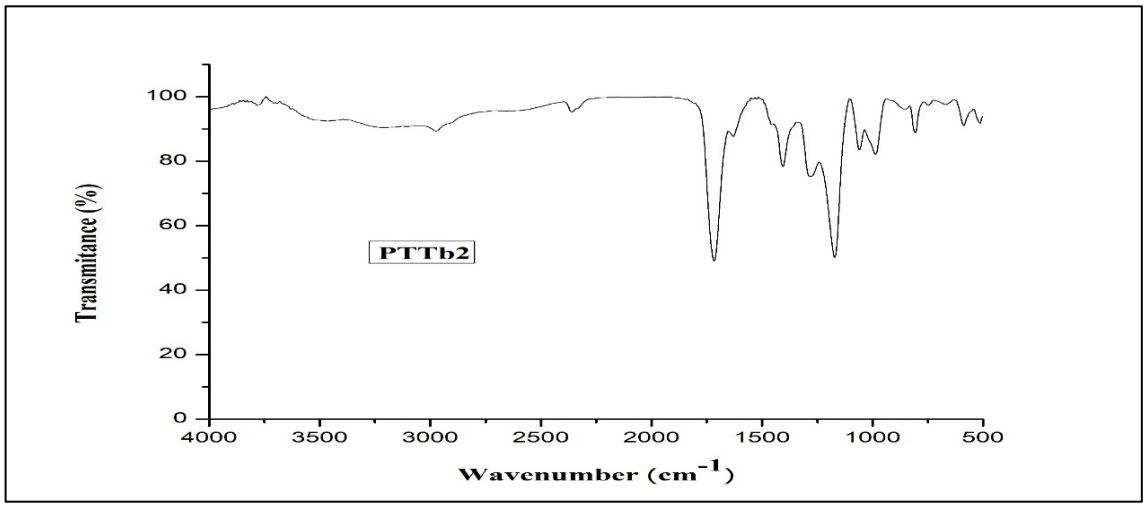

Figure 3.29: FTIR spectra of PTTb2 sample

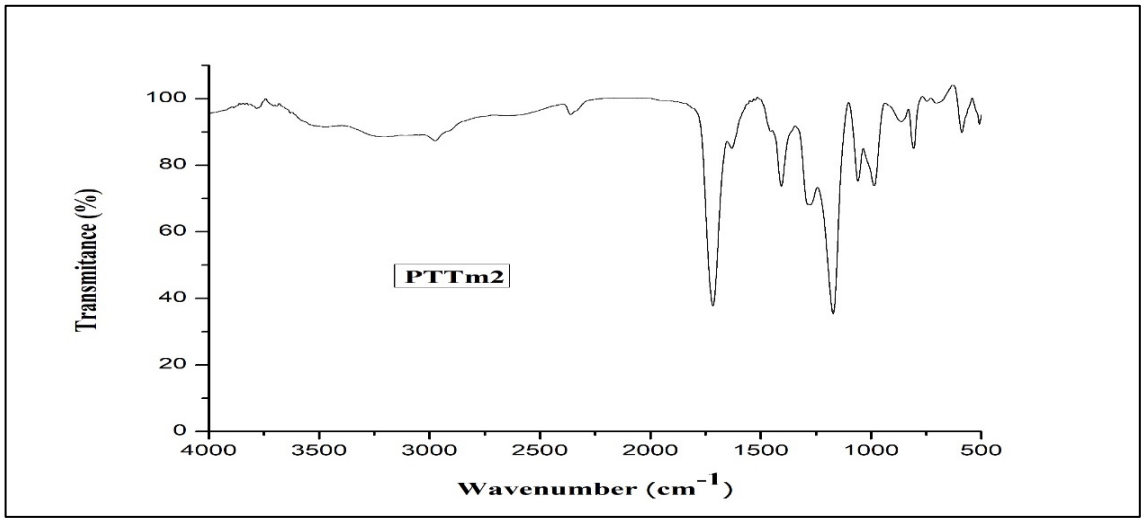

Figure 3.30: FTIR spectra of PTTm2 sample

Table 3.22: Functional group of PAA, PTRE1 and PTRE2 nanocomposites

Wavenumber (cm^{-1})	Functional group
~3420	–OH stretching vibration of water associated with the oxide matrix.
~2970	C–H stretching mode of PAA
~2360	CO_2 linearly adsorbed on the Ti^{4+} ions
~1720	C=O stretching mode of carboxylic group in PAA [11]
~1630	–OH bending mode of hydroxyl groups present on the surface due to moisture
~1460	$–COO^-$ group of PAA [11]
~1405	CH_2 bonding mode of PAA [11]
~1400 and ~590	Ti–O stretching vibrations of TiO_2 anatase phase [11]
~1170	–(C–O)H stretching mode of PAA [11]
~1060	C–CH_2 stretching mode of PAA
~980	various vibrations of the Ti-O bond [11]
~800	CH_2 rocking mode of PAA [11]
~710	Characteristics of anatase phase of TiO_2
The strong peaks in the range 500 to 1500	Ti–O vibration modes. [11]

3.4 Optical Properties:

Study of fluorescence emission of TiO_2:RE-polyacrylicacid nanocomposites was carried out by Photo-Luminescence (PL) Spectroscopy. UV-Visible Spectroscopy was used to determine the optical properties of the prepared nanocomposites.

3.4.1 Photoluminescence Spectroscopy (PL)

Photoluminescence study was done using JASCO FP-6500 spectrofluorometer. **Figure 3.31** presents the PL spectra of 1 mol% TiO_2:RE – PAA nanocomposites (PTRE1). The spectra along with that for pure PAA was recorded at 265 nm excitation wavelength. PL spectra of 2 mol% TiO_2:RE – PAA nanocomposites (PTRE2) and pure PAA recorded at 265 nm excitation wavelength is shown in **Figure 3.32**. The PL spectra exhibits wide peaks centered at 300 nm in UV emission band and other emission peaks between 380 nm to 495 nm in the violet-blue emission band, while there is no significant emission in pure PAA at 265 nm excitation.

From **Figure 3.31** and **Figure 3.32**, it can be observed that the overall emission pattern of samples in the UV and violet-blue emission bands remain almost constant. The change occurs only in intensities of PL signals at different wavelength, which can be due to the change in the density of defect levels. The emission peaks are slightly shifted with doping percentage.

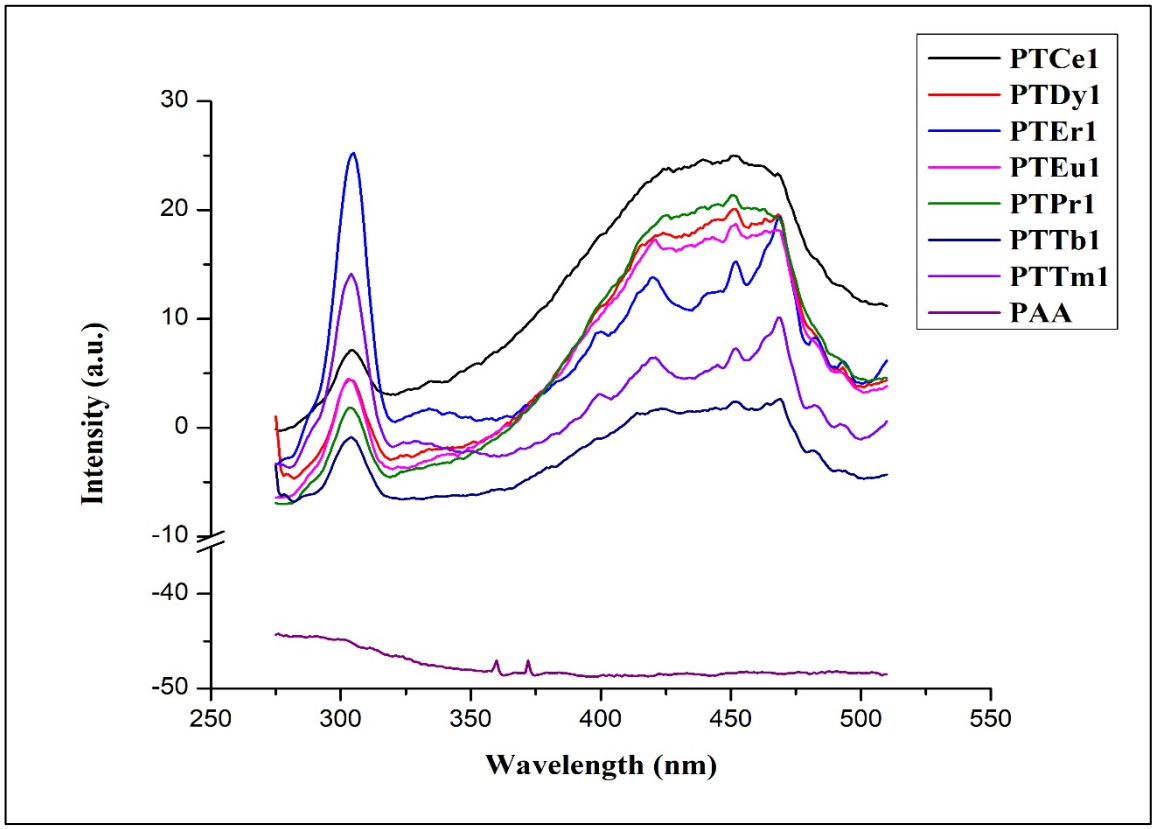

Figure 3.31: PL spectra of PTRE1 (RE= Ce, Dy, Er,Eu, Pr, Tb, Tm) samples

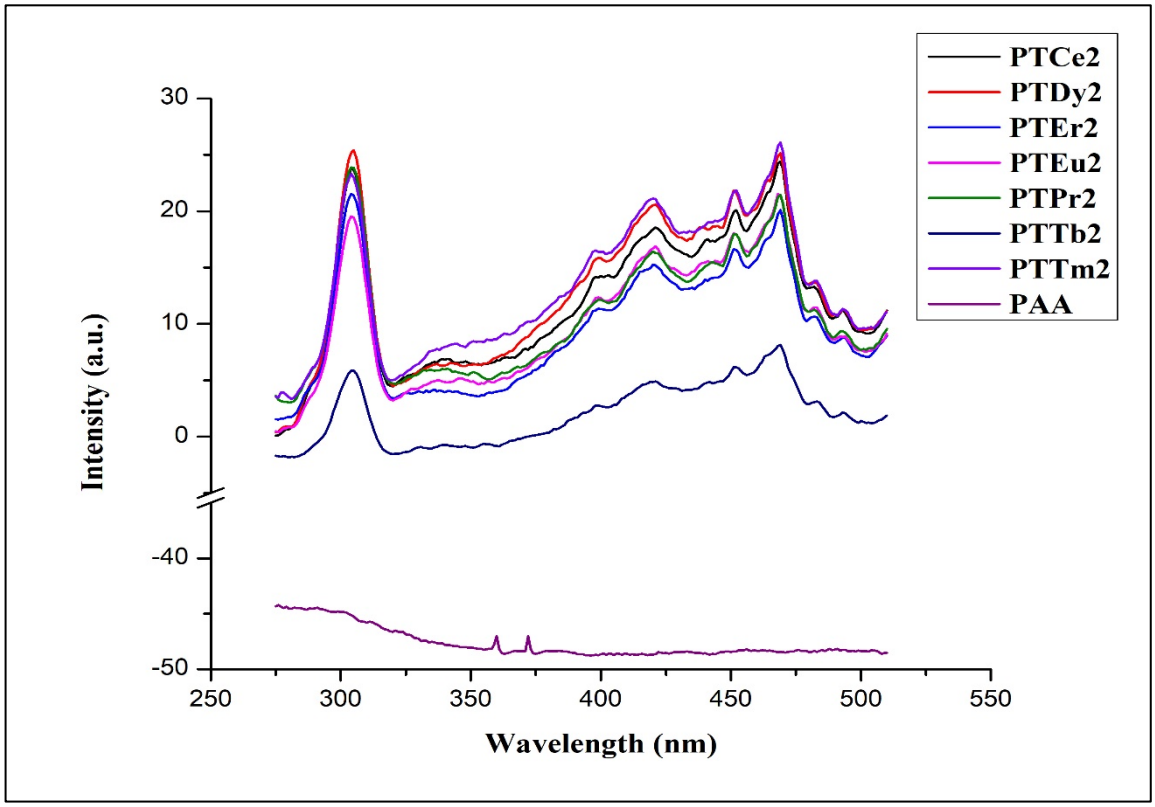

Figure 3.32: PL spectra of PTRE2 (RE= Ce, Dy, Er, Eu, Pr, Tb, Tm) samples

3.4.2 UV-Vis Spectroscopy (UV-Vis)

The optical properties of prepared samples were investigated by UV-Visible absorption spectra. UV-Visible spectroscopic studies were done using UV-3600 Shimadzu spectrometer recorded in the wavelength range 200 to 800 nm. The optical bandgap was evaluated by Tauc's plot. The UV-Visible absorption spectra and corresponding Tauc's plot of pure PAA and 1 mol% TiO_2:RE – PAA nanocomposites (PTRE1) are shown in **Figures 3.33** to **3.40**. The different optical parameters calculated from UV-Visible absorption spectra are given in **Table 3.23**.

The absorption edge of all the samples are below 325 nm. The peak absorption wavelengths vary in a range between 274 nm to 290 nm. Hence, there is no substantial change in the absorption pattern.

The optical bandgap of all the RE:TiO_2-PAA composite samples lie between 3.75 eV to 4.25 eV. The bandgap values of these composite samples are obviously higher compared to pure TiO_2 which has a band gap of 3.2 eV. The band gap of PAA studied for this work was found to be 4.34 eV. The refractive index of the samples varies in a very short range from 2.11 to 2.20. Er doped TiO_2 and Tb doped TiO_2 samples show lowest and highest refractive index respectively. This is higher in comparison to reported value of 1.395. The calculated value of refractive index for pure PAA is 2.06.

Figure 3.41 shows variation of absorption coefficient with wavelength. All the samples show higher absorption below 325 nm. After that, the absorption remains constant throughout the visible range. Dy, Eu, and Pr doped TiO_2-PAA composites show relatively higher absorption and found to be decreasing in a pattern given by PTDy1>PTEu1>PTPr1>PTCe1>PTTm1>PTEr1>PTTb1.

Figure 3.42 shows variation of extinction coefficient with wavelength. The value of extinction coefficient remains high for all the samples up to 325 nm, after which the value remains constant. The change in extinction co efficient between samples is very small and remains almost uniform throughout the visible range. There is small increase towards higher wavelength for Er and Tm doped samples.

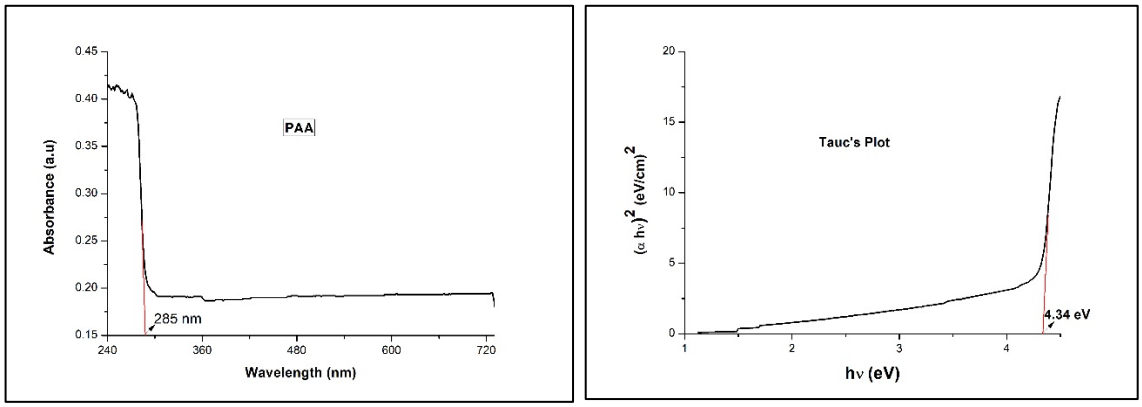

Figure 3.33: UV-Vis absorption spectra and Tauc's plot of pure PAA

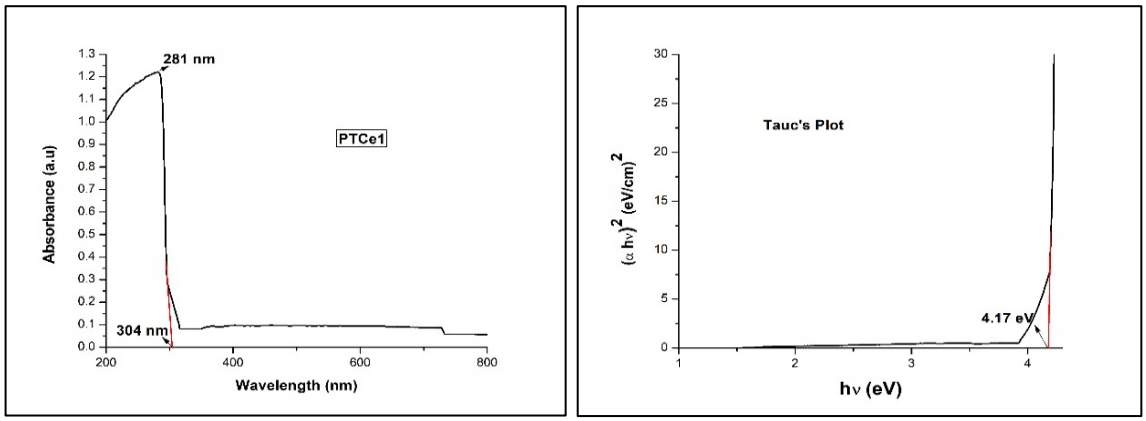

Figure 3.34: UV-Vis absorption spectra and Tauc's plot of PTCe1 sample

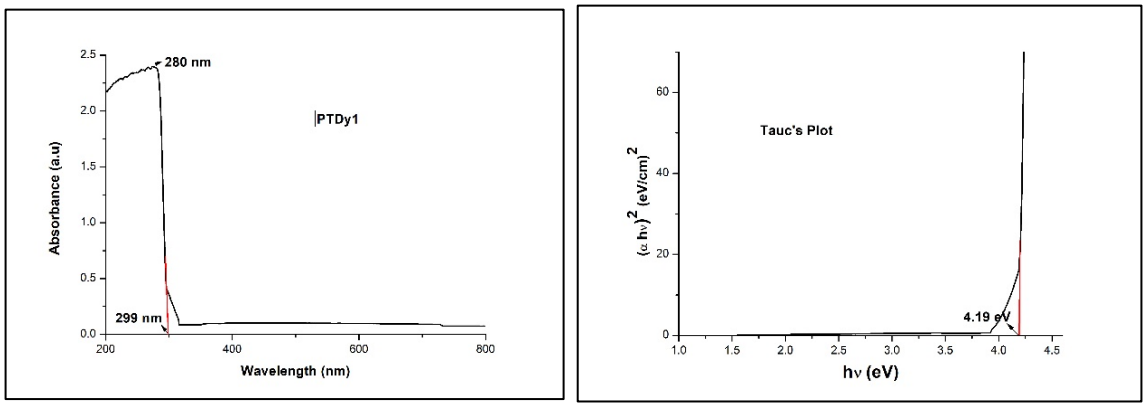

Figure 3.35: UV-Vis absorption spectra and Tauc's plot of PTDy1 sample

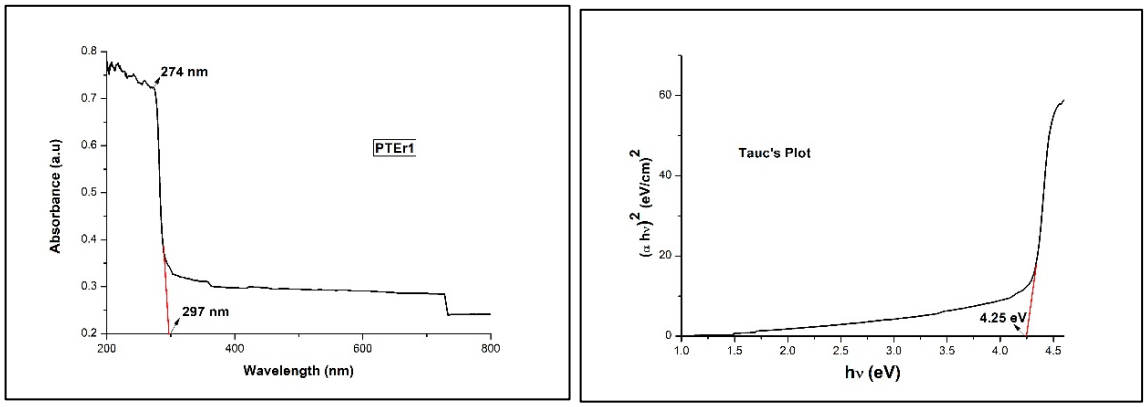

Figure 3.36: UV-Vis absorption spectra and Tauc's plot of PTEr1 sample

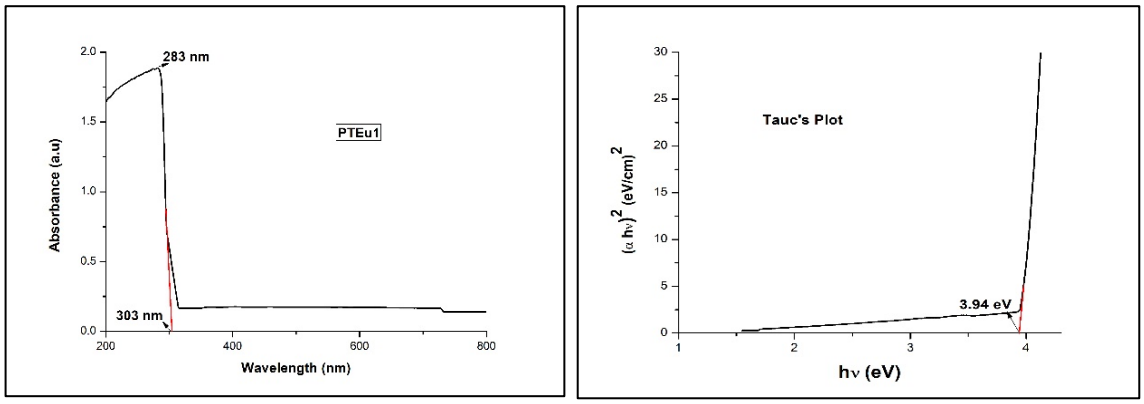

Figure 3.37: UV-Vis absorption spectra and Tauc's plot of PTEu1 sample

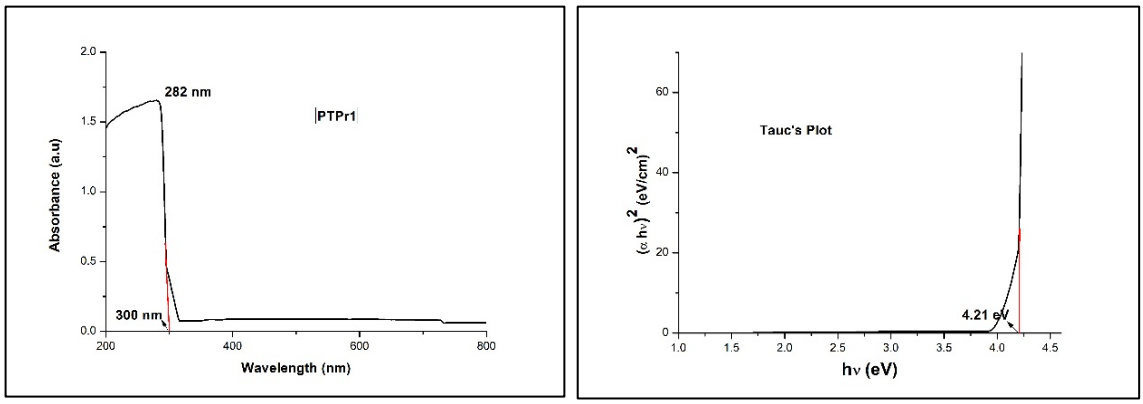

Figure 3.38: UV-Vis absorption spectra and Tauc's plot of PTPr1 sample

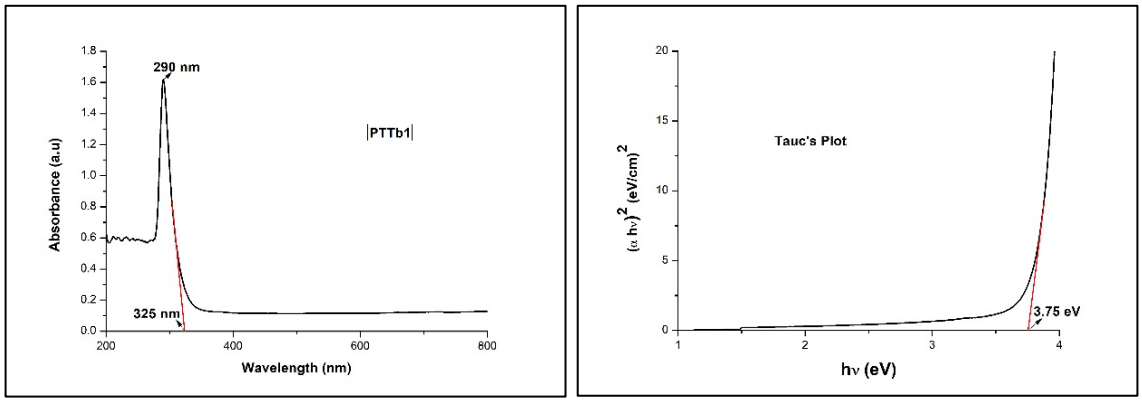

Figure 3.39: UV-Vis absorption spectra and Tauc's plot of PTTb1 sample

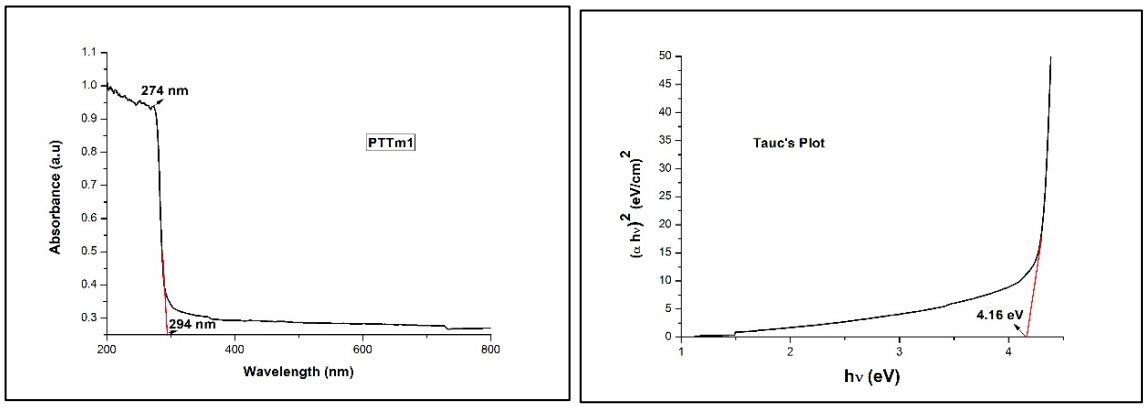

Figure 3.40: UV-Vis absorption spectra and Tauc's plot of PTTm1 sample

Table 3.23: Optical parameters of PTRE1 (RE= Ce, Dy, Er, Eu, Pr, Tb, Tm)

Sample	Peak Absorption	Optical Bandgap	Refractive Index
PAA	285	4.34 eV	2.06
PTCe1	281	4.17 eV	2.13
PTDy1	280	4.19 eV	2.12
PTEr1	274	4.25 eV	2.11
PTEu1	283	3.94 eV	2.16
PTPr1	282	4.21 eV	2.12
PTTb1	290	3.75 eV	2.20
PTTm1	274	4.16 eV	2.13

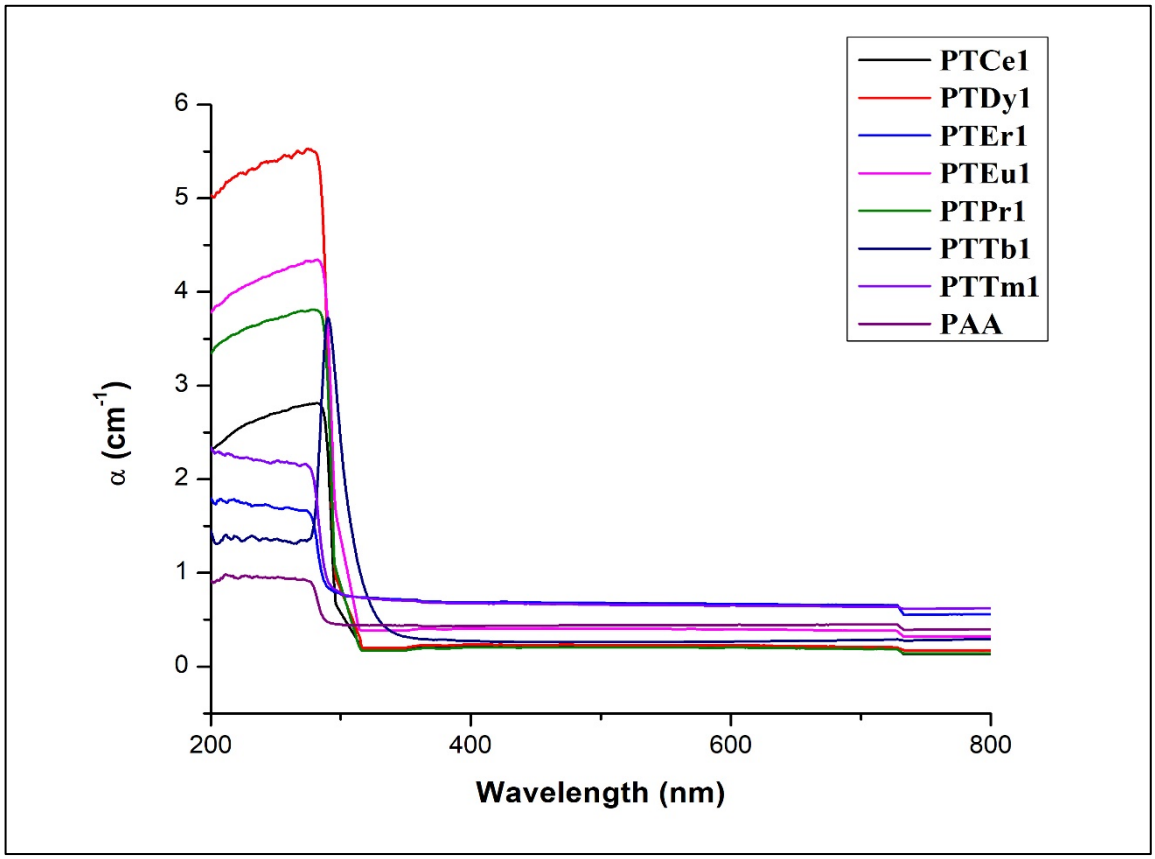

Figure 3.41: Variation of Absorption coefficient with wavelength for PTRE1

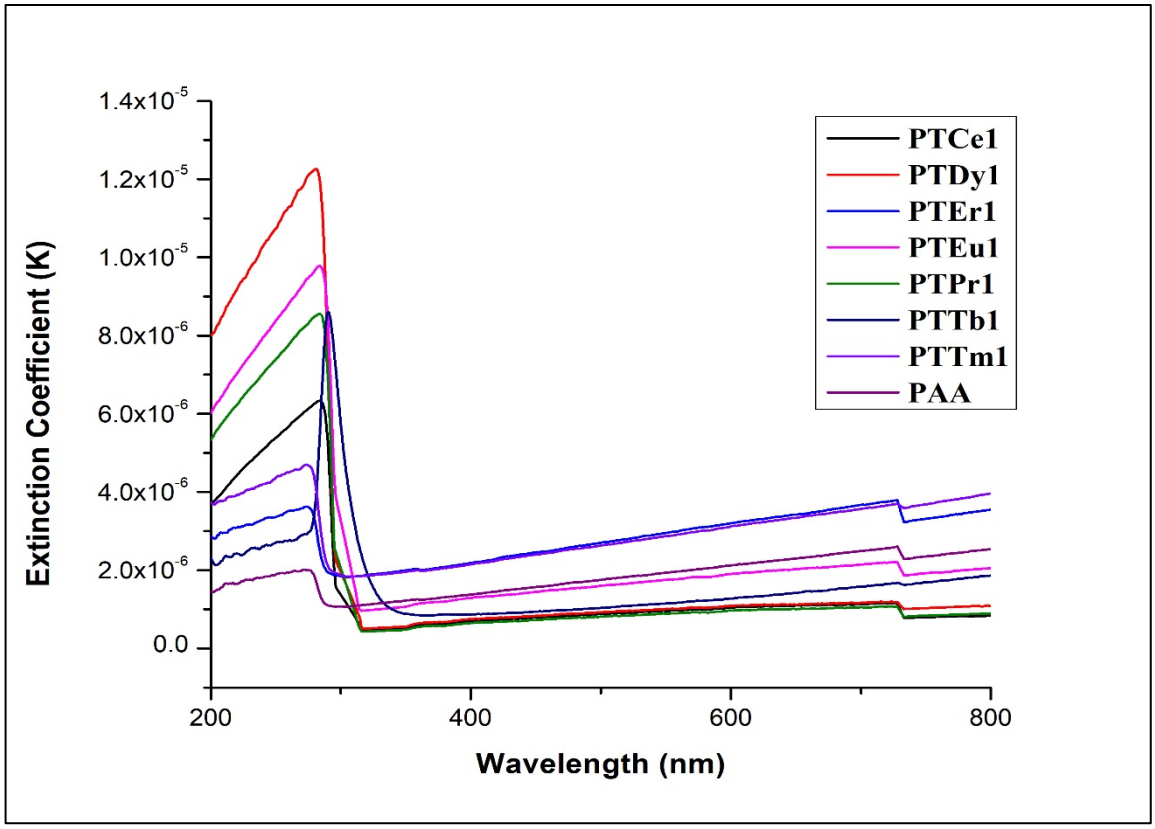

Figure 3.42: Variation of Extinction coefficient with wavelength for PTRE1

The UV-Visible absorption spectra and corresponding Tauc's plot of 2 mol% TiO_2:RE – PAA nanocomposites (PTRE2) are shown in **Figures 3.43** to **3.49**. The different optical parameters calculated from UV-Visible absorption spectra are given in **Table 3.24**.

The absorption edge of all the samples lies below 318 nm. The peak absorption wavelengths vary in a range between 274 nm to 293 nm. Hence, there is no substantial change in the absorption pattern. The optical bandgap of all the samples lie between 3.82 eV to 4.30 eV.

The refractive index of the samples vary in a very short range from 2.10 to 2.19. Er doped TiO_2 and Tb doped TiO_2 samples show lowest and highest refractive index respectively.

Figure 3.50 shows variation of absorption coefficient with wavelength. All the samples show higher absorption below 315 nm. After that, the absorption remains constant. Dy, Er and Eu doped TiO_2-PAA composites show relatively higher absorption and found to be decreasing in a pattern given by PTDy2>PTEr2>PTEu2>PTTm2>PTCe2>PTPr2>PTTb2. However, it is lower than the samples with 1 mole % blending.

Figure 3.51 shows variation of extinction coefficient with wavelength. The value of extinction coefficient remains high for all the samples below 315 nm. The change in extinction co efficient for samples is very small and remains almost uniform throughout the entire range. The values of extinction coefficient rise towards the visible region and near IR. The values are highest for Ce and Tm doped samples.

Hence, PTRE1 set of samples show higher absorption of UV in comparison to PTRE2 samples.

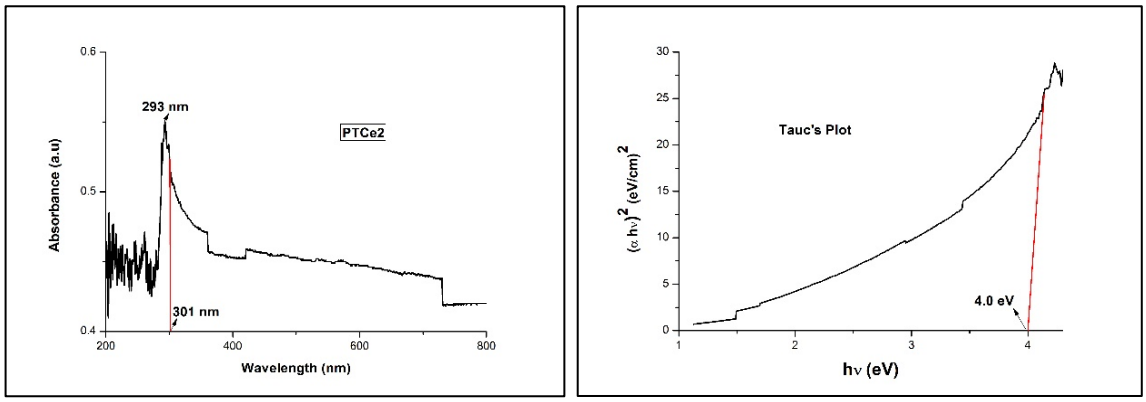

Figure 3.43: UV-Vis absorption spectra and Tauc's plot of PTCe2 sample

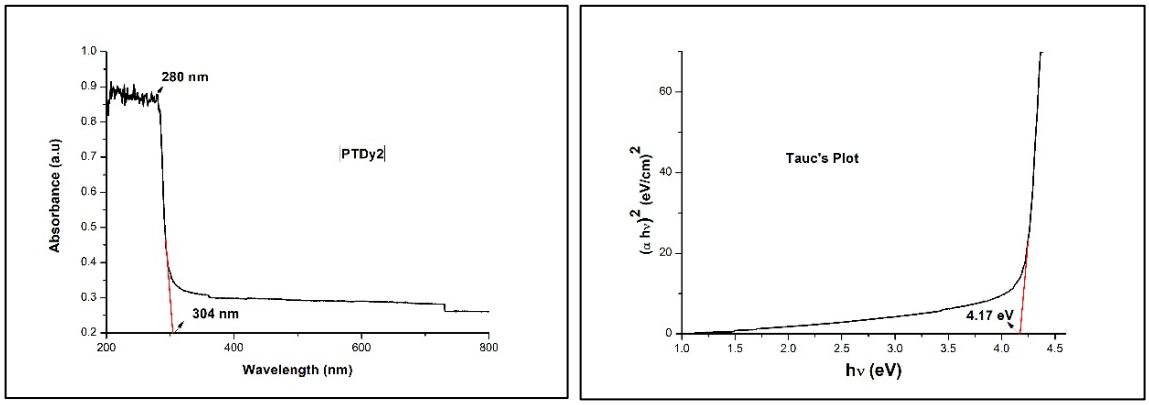

Figure 3.44: UV-Vis absorption spectra and Tauc's plot of PTDy2 sample

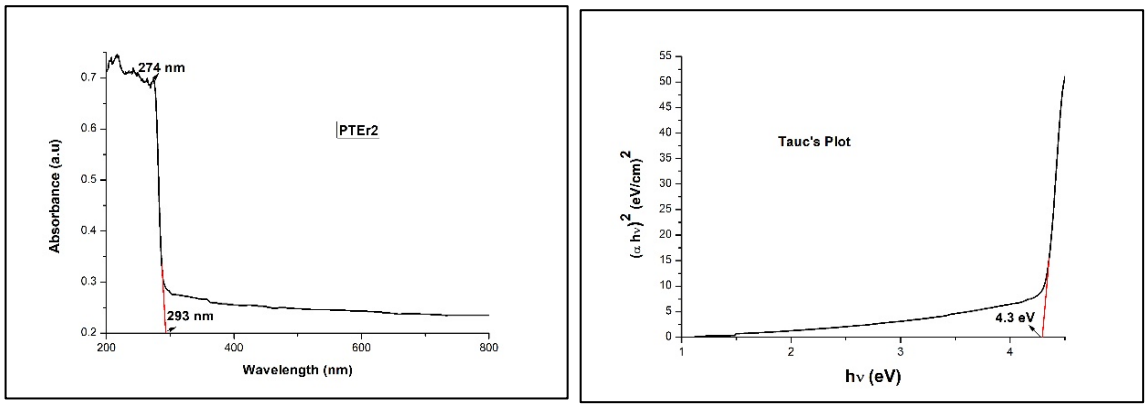

Figure 3.45: UV-Vis absorption spectra and Tauc's plot of PTEr2 sample

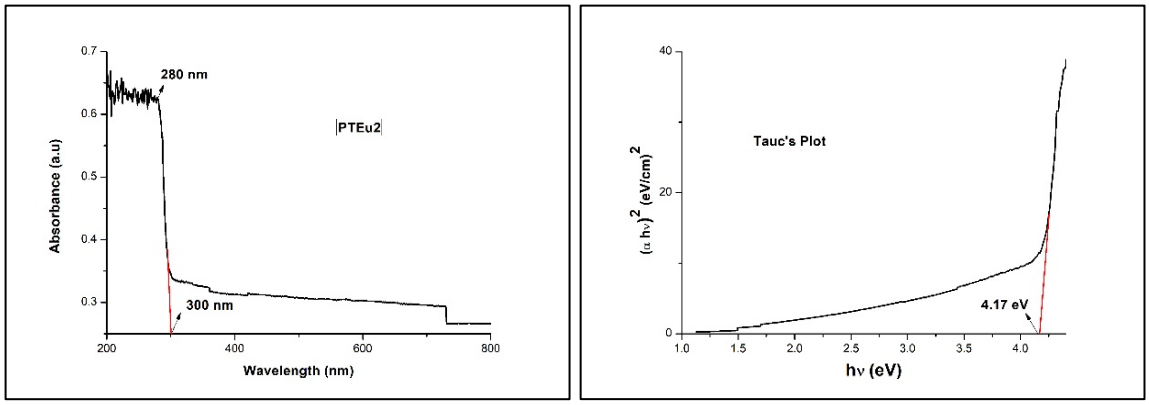

Figure 3.46: UV-Vis absorption spectra and Tauc's plot of PTEu2 sample

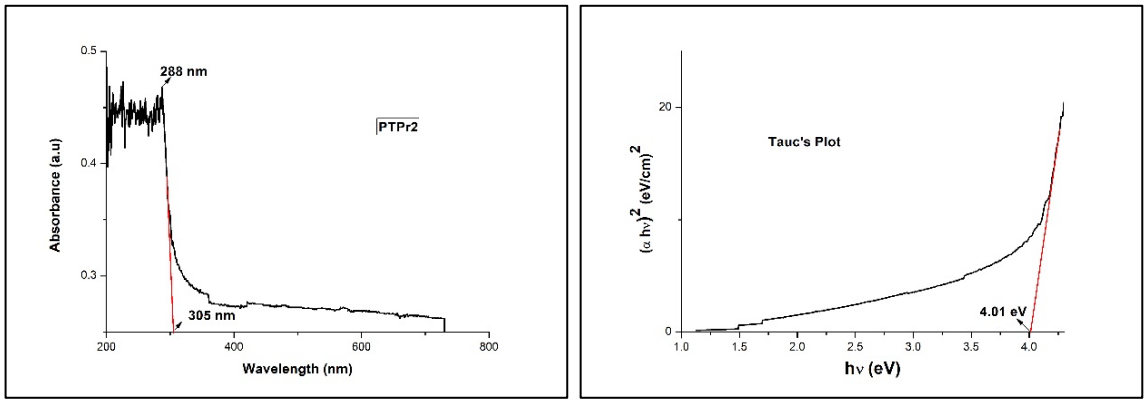

Figure 3.47: UV-Vis absorption spectra and Tauc's plot of PTPr2 sample

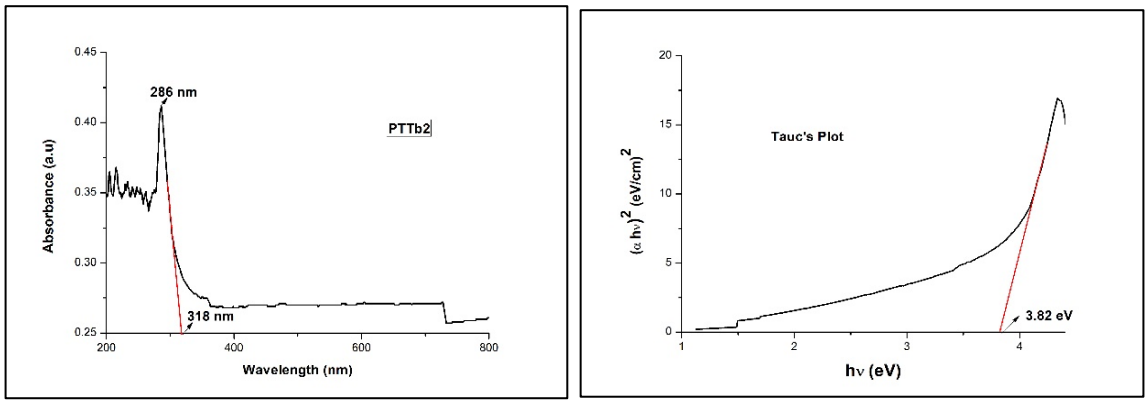

Figure 3.48: UV-Vis absorption spectra and Tauc's plot of PTTb2 sample

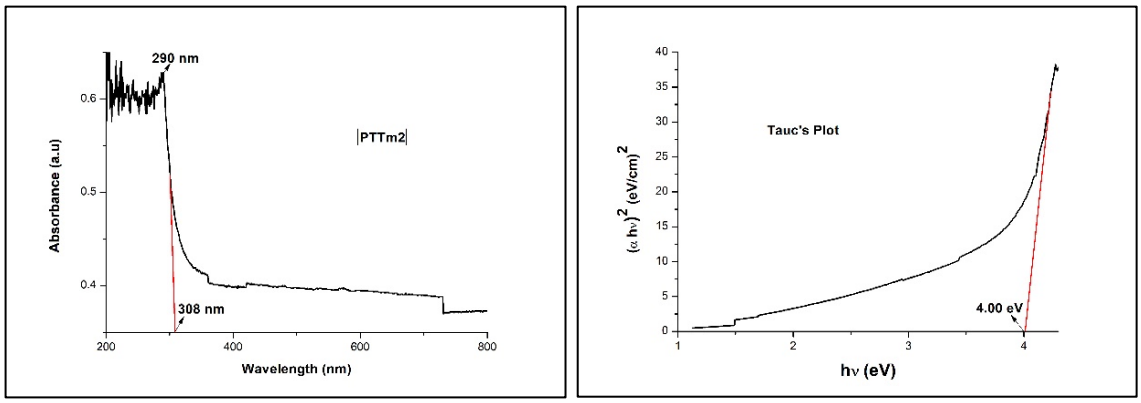

Figure 3.49: UV-Vis absorption spectra and Tauc's plot of PTTm2 sample

Table 3.24: Optical parameters of PTRE2 (RE= Ce, Dy, Er, Eu, Pr, Tb, Tm)

Sample	Peak Absorption	Optical Bandgap	Refractive Index
PAA	285	4.34 eV	2.06
PTCe2	293	4.00 eV	2.15
PTDy2	280	4.17 eV	2.13
PTEr2	274	4.30 eV	2.10
PTEu2	280	4.17 eV	2.13
PTPr2	288	4.01 eV	2.15
PTTb2	286	3.82 eV	2.19
PTTm2	290	4.00 eV	2.15

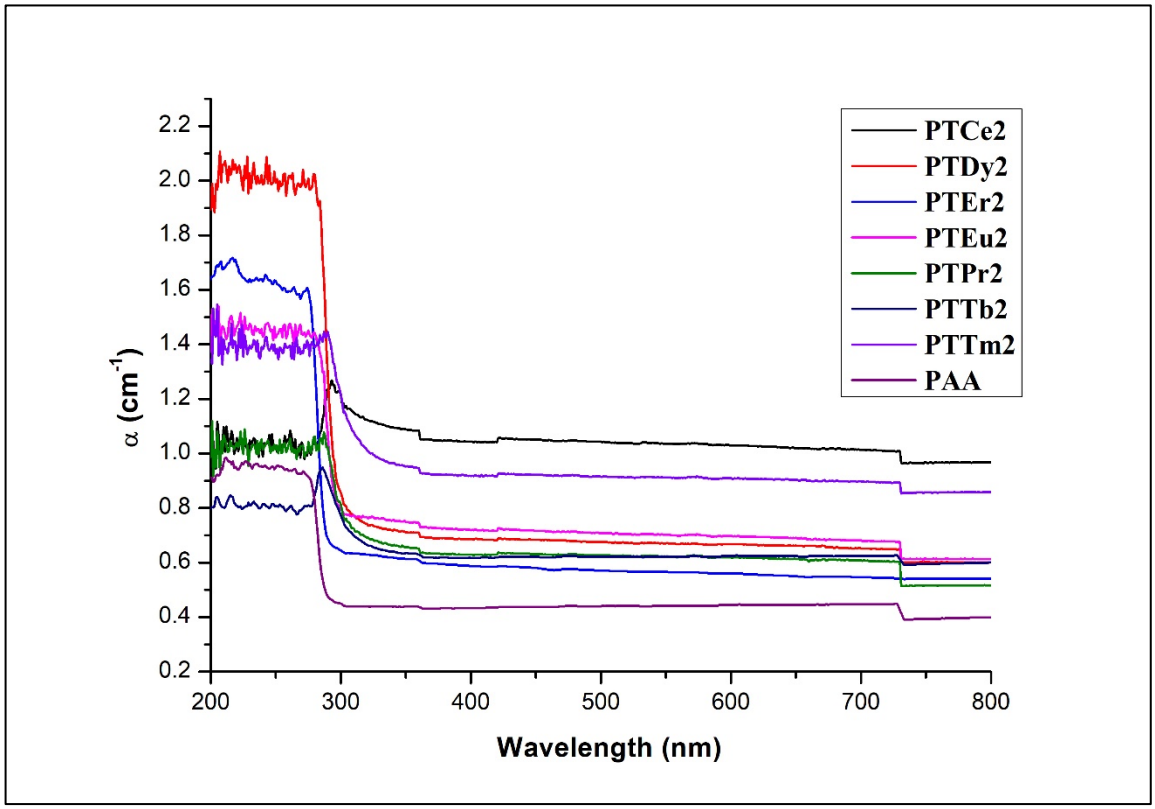

Figure 3.50: Variation of Absorption coefficient with wavelength for PTRE2

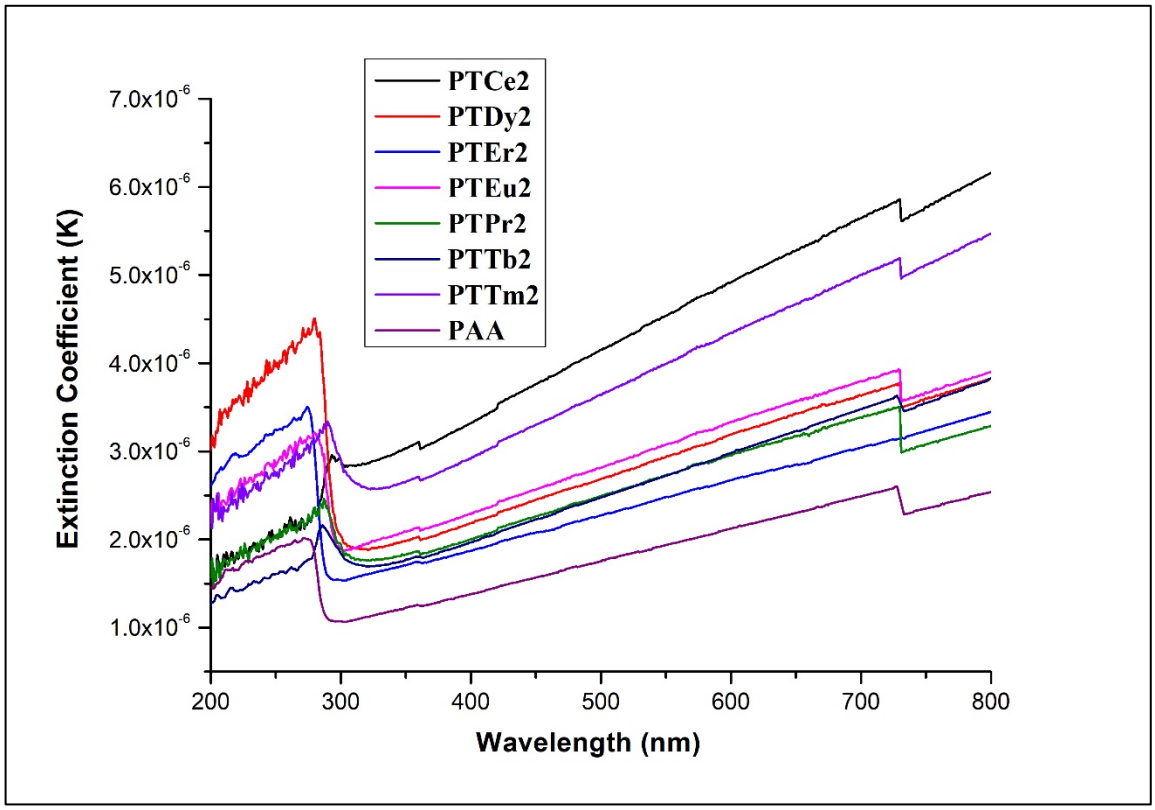

Figure 3.51: Variation of Extinction coefficient with wavelength for PTRE2

3.5 Summary:

Rare earth doped TiO_2 – PAA nanocomposites were prepared using hydrothermal method and doctor blade method. The XRD results revealed the formation of material as nano crystallite and confirms the material structure formation and it matches with the standard JCPDS results. DLS results give particle size distribution in nano meters. The EDS spectra of samples indicate the presence of Titanium, Oxygen and rare earth elements. The FTIR spectra confirms the presence of different functional groups with respective wavenumber for PAA. The Photoluminescence study exhibits wide peaks in UV region and violet-blue region.

The optical properties of material were analysed by UV- Visible Spectroscopy. The bandgap values of the composites are between that of pure TiO_2 and pure PAA. The refractive index is higher than pure PAA. The variation of absorption coefficient with wavelength shows higher absorption in UV range. The value of extinction coefficient is high for all the samples below 315 nm. PTRE1 (1 mol%) set of samples show higher absorption of UV in comparison with PTRE2 (2 mol%) samples.

References:

[1] A.P. Oliveira, M.L. Torem, The influence of precipitation variables on zirconia powder synthesis, Powder Technol. 119 (2001) 181–193.

[2] C. Stocker, A. Baiker, Zirconia aerogels: effect of acid-to-alkoxide ratio alcoholic solvent and supercritical drying method on structural properties, J. Non-Cryst. Solids 223 (1998) 165–178.

[3] V.V. Srdic, M. Winterer, Comparison of nanosized zirconia synthesized by gas and liquid phase methods, J. Eur. Ceram. Soc. 26 (2006) 3145–3151.

[4] R.D. Purohit, S. Saha, A.K. Tyagi, Combustion synthesis of nanocrystalline ZrO2 powder: XRD Raman spectroscopy and TEM studies, Mater. Sci. Eng. B 130 (2006) 57–60.

[5] M. Gateshki, V. Petkov, G. Williams, S.K. Pradhan, Y. Ren, Atomic-scale structure of nanocrystalline ZrO2 prepared by high-energy ball milling, Phys. Rev. B 71 (2005) 224107–2241016.

[6] W. Pyda, K. Haberko, M.M. Bucko, Hydrothermal crystallization of zirconia and zirconia solid solution, J. Am. Ceram. Soc. 74 (1991) 2622–2629.

[7] Aytaç ŞAHİN, İzmir Institute of Technology, İzmir, Turkey İzmir, Institute of Technology, İzmir, (2004) Turkey.

[8] Wojciech L. Suchanek1 and Richard E. Riman, Hydrothermal Synthesis of Advanced Ceramic Powders, Advances in Science and Technology 45 (2006) 184-193.

[9] JCPDS-ICDD, Joint committee for powder diffraction standards, International Center of Diffraction Data (1997).

[10] A. L. Patterson, “The Scherrer Formula for X-Ray Particle Size Determination”, Phys. Rev., 56 (1939), pp. 978.

[11] Chiam-Wen Liew, H.M. Ng, Arshid Numan, S. Ramesh, Poly(Acrylic acid)–Based Hybrid Inorganic–Organic Electrolytes Membrane for Electrical Double Layer Capacitors Application, Polymers 8, 179 (2016).